HYDROGEN EMBRITTLEMENT OF NICKEL

Technical Report

October 1984

D. Lassila and H.K. Birnbaum

University of Illinois
Department of Metallurgy
Urbana, IL 61801

DTIC
ELECTE
S D
DEC 7 1984
D

This document is unclassified. Reproduction and distribution for any purpose of the U.S. government is permitted.

84 11 08 049

SECURITY CLASSIFICATION OF THIS PAGE *(When Data Entered)*

REPORT DOCUMENTATION PAGE		READ INSTRUCTIONS BEFORE COMPLETING FORM
1. REPORT NUMBER	**2. GOVT ACCESSION NO.**	**3. RECIPIENT'S CATALOG NUMBER**
4. TITLE *(and Subtitle)* Hydrogen Embrittlement of Nickel		**5. TYPE OF REPORT & PERIOD COVERED** Technical
		6. PERFORMING ORG. REPORT NUMBER
7. AUTHOR(s) D. Lassila and H.K. Birnbaum		**8. CONTRACT OR GRANT NUMBER(s)** N-00014-83-K-0468
9. PERFORMING ORGANIZATION NAME AND ADDRESS University of Illinois Dept. of Metallurgy 1304 W. Green St., Urbana, Il 61801		**10. PROGRAM ELEMENT, PROJECT, TASK AREA & WORK UNIT NUMBERS**
11. CONTROLLING OFFICE NAME AND ADDRESS Office of Naval Research Arlington, VA 22200		**12. REPORT DATE** October, 1984
		13. NUMBER OF PAGES
14. MONITORING AGENCY NAME & ADDRESS*(if different from Controlling Office)*		**15. SECURITY CLASS.** *(of this report)*
		15a. DECLASSIFICATION/DOWNGRADING SCHEDULE

16. DISTRIBUTION STATEMENT *(of this Report)*

This document is unclassified. Reproduction and distribution for any purpose of the U.S. government is permitted.

17. DISTRIBUTION STATEMENT *(of the abstract entered in Block 20, if different from Report)*

18. SUPPLEMENTARY NOTES

19. KEY WORDS *(Continue on reverse side if necessary and identify by block number)*

Hydrogen Embrittlement   Solute Segregation
Nickel
Fracture

20. ABSTRACT *(Continue on reverse side if necessary and identify by block number)*

(over)

HYDROGEN EMBRITTLEMENT OF NICKEL

D.H. Lassila, H.K. Birnbaum

Experiments were performed to determine the effects of hydrogen segregation at grain boundaries on intergranular fracture of charged nickel deformed in tension. Two modes of hydrogen segregation are investigated; lattice diffusion and dislocation transport of Cottrell atmospheres of hydrogen.

The results of this study show that the parameters affecting the diffusive segregation of hydrogen to grain boundaries play a fundamental role in conditions which result in embrittlement. If a sufficient quantity of hydrogen at grain boundaries is attained, the fracture mode of nickel will change from ductile rupture to intergranular. Experiments performed to evaluate the role of dislocation transport of hydrogen in the embrittlement of nickel suggest that dislocation transport has no effect on embrittlement at temperatures below 208 K. However, at 300 K the observed strain rate dependence on fracture behavior suggests dislocation transport causes nonequilibrium hydrogen segregation at grain boundaries.

An analysis of the thermodynamics and kinetics of hydrogen segregation yielded values for the binding enthalpy of hydrogen to nickel grain boundaries and the breadth of hydrogen enhancement at boundaries. By considering these values and other test results two separate mechanistic contributors of hydrogen embrittlement of charged nickel are proposed.

HYDROGEN EMBRITTLEMENT OF NICKEL

David H. Lassila, Ph.D.
Department of Metallurgy and Mining Engineering
University of Illinois at Urbana-Champaign, 1984

Experiments were performed to determine the effects of hydrogen segregation at grain boundaries on intergranular fracture of charged nickel deformed in tension. Two modes of hydrogen segregation are investigated; lattice diffusion and dislocation transport of "Cottrell atmospheres" of hydrogen. The effect of cosegregation of hydrogen and sulfur is also explored.

The results of this study show that the parameters affecting the diffusive segregation of hydrogen to grain boundaries play a fundamental role in conditions which result in embrittlement. If a sufficient quantity of hydrogen at grain boundaries is attained, the fracture mode of nickel will change from ductile rupture to intergranular. Experiments performed to evaluate the role of dislocation transport of hydrogen in the embrittlement of nickel suggest that dislocation transport has no effect on embrittlement and that the embrittlement mechanism is not dependent on hydrogen mobility.

An analysis of the thermodynamics and kinetics of hydrogen segregation yielded values for the binding enthalpy of hydrogen to nickel grain boundaries and the breadth of hydrogen enhancement at boundaries. By considering these values and other test results a mechanism of hydrogen embrittlement of nickel is proposed.

Three series of nickel tensile specimens were tested with various amounts of sulfur segregation present at grain boundaries. Segregation on the order of 0.1 monolayer has been shown to severely increase the embrittlement susceptibility of hydrogen charged nickel.

TABLE OF CONTENTS

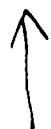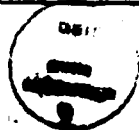Accession For

NTIS GRA&I   ✗
DTIC TAB   ☐
Unannounced   ☐
Justification

By Per Ltr. on file

Distribution/

Availability Codes

	Avail and/or	
Dist	Special	
A/1		

1

INTRODUCTION

The harmful effect of hydrogen on the mechanical properties of nickel is worthy of scientific study for the sake of academic knowledge as well as for the alleviation of engineering problems which arise when structural components made of nickel or nickel base alloys are exposed to hydrogen. It is a well documented fact that solute hydrogen considerably reduces the ductility of nickel in a tensile test. This reduction in ductility of relatively pure polycrystalline nickel is accompanied by a change in fracture mode from ductile microvoid coalescence to intergranular fracture[1-6]. In essence premature failure occurs due to the intervention of grain boundary fracture. Much speculation and effort has been put forth to explain the observed embrittlement and several mechanisms have been invoked. Controversy is often centered on the observed test temperature and strain rate dependence of embrittlement as well as on differences in test material and other parameters between different studies.

In this work the effect of hydrogen segregation at grain boundaries on intergranular fracture is studied. Two modes of hydrogen segregation are investigated; lattice diffusion and dislocation transport of "Cottrell atmospheres" of hydrogen. The effect of cosegregation of hydrogen and sulfur is also explored.

Several studies suggest that considerable hydrogen segregation at nickel grain boundaries can occur via lattice diffusion[7,8]. The thermodynamics of hydrogen segregation and the kinetics of hydrogen transport in the lattice will have a large impact on the enhancement of the hydrogen concentration at boundaries. Assuming a negative binding enthalpy between a hydrogen atom and a grain boundary

trapping site, as the thermal energy of the material is lowered, a greater percentage of trap sites will be filled provided they are not saturated. However, at the same time transport of hydrogen to trap sites will slow because of the positive activation energy for diffusion. To study the effect of diffusive segregation of hydrogen to grain boundaries on embrittlement of nickel, hydrogen charged material was aged at various temperatures for various periods to allow the accumulation of solute hydrogen at boundary trap sites. The material was then quenched and tested under conditions such that hydrogen distributions obtained by aging would be essentially unaltered and the effect of segregation alone could be determined. The results of this study show that the parameters affecting the diffusion of hydrogen to grain boundaries play a fundamental role in conditions which result in embrittlement and also explain the test temperature and strain rate dependence reported in other studies.

Several authors have suggested that dislocation transport of hydrogen in nickel plays a major role in embrittlement i.e. grain boundary fracture[2,9]. To study the effect of hydrogen transport by dislocations on the fracture mode of nickel, testing was performed at a temperature that is expected to enhance dislocation transport (-65°C), provided a critical strain rate ($\sim 10^{-4} \, \text{sec}^{-1}$) is not exceeded. Two strain rates were employed for this study, one faster than that critical strain rate so that dislocation transport will not occur and one slower so that dislocation transport will occur. The results of these tests revealed that there is no effect of strain rate and presumably of dislocation transport on the fracture mode and that the fracture behavior at -65°C was essentially the same as that at -198°C for a given degree of hydrogen enhancement at grain boundaries.

It has been known for some time that sulfur segregation at nickel grain boundaries can cause intergranular fracture resulting in a severe decrease of ductility[10]. In this study it is shown that about one tenth monolayer of sulfur coverage will cause a dramatic increase in the propensity of intergranular fracture of hydrogenated nickel.

Literature that pertains to this work and fundamentals of the behavior of hydrogen in nickel are reviewed in the first chapter. This is followed by chapters which describe experimental procedures and results. A qualitative analysis of some results is performed in Chapter 4 which yields a value for the binding enthalpy of hydrogen to nickel grain boundaries and other information concerning hydrogen segregation. Discussion of the results of this work and hydrogen embrittlement of nickel in general is given in Chapter 5.

CHAPTER 1

LITERATURE SURVEY

Literature that pertains to the goals of this work is reviewed in the following chapter. Where appropriate, numerical values are calculated which will be used in subsequent analyses.

1.1 Hydrogen Embrittlement of Nickel

The effects of environmental and internal hydrogen on the mechanical properties, particularly fracture, of nickel are reviewed in this section. The main focus will be on the effects of internal or solute hydrogen.

1.1.1 Environmental Hydrogen

The intergranular fracture of nickel tensile specimens tested in a hydrogen environment (gaseous hydrogen[11], or tested and simultaneously cathodic charged[12]) is known to have a strong dependence on the extent of sulfur segregation at grain boundaries. Many studies[13] have shown that material heat treated to purposely segregate sulfur at grain boundaries exhibits predominantly intergranular fracture when tested in tension in hydrogen gas, while in the absence of sulfur segregation transgranular fracture predominates. It has been suggested that sulfur as well as other metalloids such as antimony act as hydrogen recombination poisons[12]. If this is true, preferential absorption occurs which essentially increases the hydrogen fugacity at the grain boundaries and which will in turn promote hydrogen assisted fracture.

Environmental hydrogen embrittlement effects are also manifested in transgranular fracture of nickel. In papers by Kamdar[14] and Chandler et al[15] the notch sensitivity of single crystal and polycrystalline samples is reported to be increased at room temperature in the presence of gaseous hydrogen and to be further increased with increasing hydrogen pressure.

1.1.2 Internal Hydrogen

a) Deformation effects

Several investigations spanning the last two decades have been undertaken to study the effect of solute hydrogen on the deformation as well as the fracture of charged nickel. In the early 60's Smith and co-workers[~,16] performed tensile tests on thermally and cathodic charged polycrystalline samples. Their results showed that the reductions in macroscopic ductility due to solute hydrogen are sensitive to strain rate, grain size, test temperature and hydrogen concentration. Some of these effects are shown graphically in Figure 1. In addition they found that solute hydrogen has a pronounced effect on the rate of work hardening and produces the Portevin-LeChatelier phenomenon (P-LCH) (serrated yielding) in the temperature range 0 to -120°C. An increase in planar slip was also reported to occur in this temperature range and was documented by SEM photographs of sides of deformed specimens and TEM photographs of specimens strained 10% in tension.

It was reasoned that the deformation behavior observed was due to the interaction of hydrogen with stationary and moving dislocations. The binding energy of a hydrogen atom to a dislocation was calculated to be about 0.08 eV based on the dependence of the P-LCH effect on test temperature and strain rate[1].
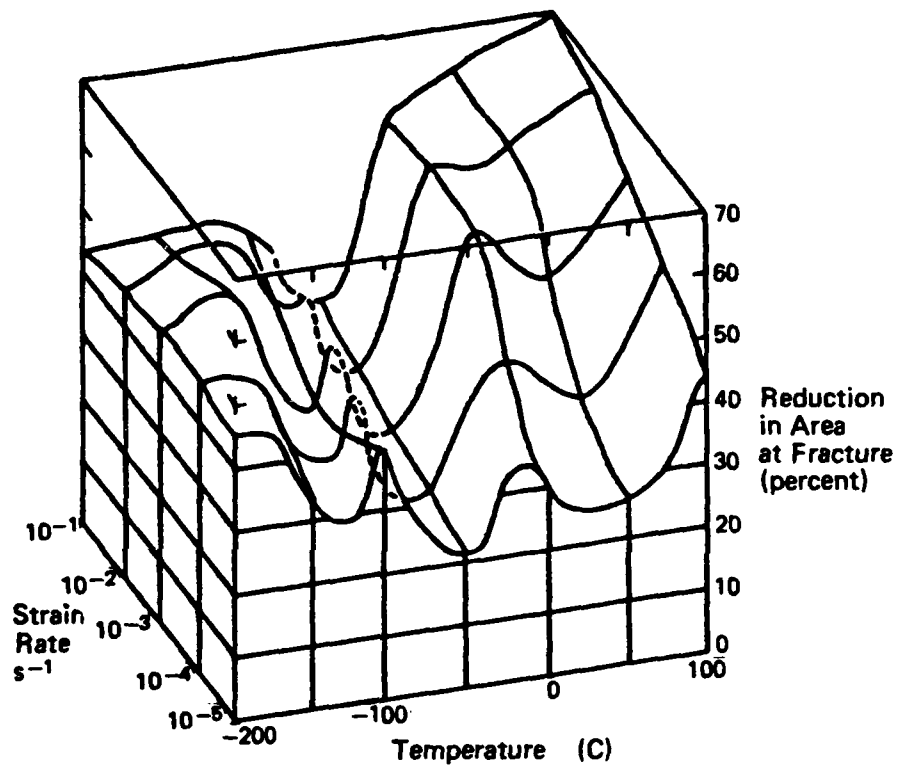
Figure 1.   The effect of strain rate and test temperature on embrittlement
of hydrogen charged nickel (after Boniszewski and Smith).

Windle and Smith[4] tested thermally charged nickel single crystals over the temperature range -198°C to 100°C. As in the case of polycrystalline samples the presence of solute hydrogen caused serrated yielding between 0°C and -120°C. Hydrogen also caused an increase in planar slip and τ_{III}. By analyzing the effect of hydrogen on τ_{III} as a function of temperature, the stacking fault energy of hydrogen charged nickel was estimated to be reduced by a factor of 0.65. This result is consistent with the reported increase in planar slip when serrated yielding is occurring eg. when hydrogen interacts with mobile dislocations.

b) Fracture

Windle and Smith[5] reported that thermally charged polycrystalline nickel tensile specimens (grain size 140 μm) containing 0.05 at.% hydrogen were embrittled when tested over the temperature range -196°C to room temperature, with maximum embrittlement occurring at an intermediate temperature range (0°C to -100°C). In another study Boniszewski and Smith[1] tested cathodically charged specimens (grain size 35 μm) containing 0.20 at.% hydrogen. Grain boundary fracture occurred at room temperature and down to approximately -120°C. Below -120°C the fracture mode reverted to ductile microvoid coalescence. At -196°C the fracture was found to be identical to that of hydrogen free samples (ductile microvoid coalescence) and was independent of strain rate. However metallographic examination revealed internal cracks which did not propagate.

The aforementioned hydrogen charged specimens were found to have prominent slip lines in the vicinity of grain boundaries that indicated a great degree of localized deformation occurred prior to fracture. The localized shear strain decreased in intensity with decreasing test temperature

but was still visible on the surface of specimens tested at -196°C. Such behavior was not reported to occur in hydrogen free samples.

Heubaum[6] examined the mechanisms of intergranular cracking of hydrogen charged nickel utilizing a low temperature tensile stage built for a scanning electron microscope. Video tapes made of the fracture process in situ showed that the intergranular "cracking" process involves a considerable amount of localized grain boundary shearing along with general deformation. Secondary cracks were found to nucleate ahead of the main crack and often linked together as straining continued.

1.2 Mechanisms of Hydrogen Assisted Fracture

Hydrogen-assisted fracture mechanisms appearing in the literature can, for the most part, be placed into one of the following subcategories;

    a) hydride formation

    b) high pressure bubble formation

    c) lattice decohesion/surface adsorption

    d) plastic deformation effects

Each of these constitutes a valid mechanism of hydrogen embrittlement in certain cases and in some instances one of the four is widely accepted as "the mechanism." For example, the embrittlement of known hydride forming metals such as Nb or Ti occurs by mechanism a). However, up to this time no single embrittlement mechanism for nickel has been accepted. In fact all four have been proposed at some time or another. The following sections will outline these mechanisms as they relate to nickel.

1.2.1 Hydride formation

Nickel hydride has been reported to be hard and brittle[17], very unlike the behavior of pure nickel which remains extremely ductile even at low temperatures. Hydride precipitation in nickel can occur in the presence of high pressure hydrogen gas (10,000 atm. or greater) or during cathodic charging procedures when high hydrogen overpotentials are employed. It has been shown that the decomposition of the nickel hydride phase and subsequent desorption of hydrogen results in the formation of microcracks[12] which have been reported to occur on {100} crystallographic planes. These surfaces are similar to fracture surfaces of metals known to be embrittled by hydride phases (Nb, Ti)[18]. Thus, under conditions of extremely high hydrogen fugacities, hydride formation is a probable embrittlement mechanism.

Hydride precipitation in metals with a positive heat of solution (equilibrium solubility decreases with decreasing temperature) is possible upon quenching from high temperatures in hydrogen gas (thermal charging). Wayman et al[19] performed tensile tests on several fcc nickel-iron alloys that were charged thermally by heating in one atmosphere of dried hydrogen at 1000°C for 1 hour and then quenched into ice water. It had been shown[20] that iron when added to nickel in solid solution reduces the stability of hydride phases in the nickel-iron system. Based on the correlation of hydride stability and embrittlement, it was suggested that the observed embrittlement of these specimens was associated with the grain boundary precipitation of a hydride which decomposes during or after fracture. However no direct observation of the hydride phase had been made before or after testing was performed.

1.2.2 High pressure bubble formation

It has been suggested that high hydrogen gas pressure can induce and provide a driving force for crack propagation[21]. High internal gas pressures in voids may result from the egress of dislocations with associated Cottrell atmospheres of hydrogen, desorption of hydrogen in a supersaturated nickel-hydrogen solution, or the decomposition of a hydride phase. This mechanism is generally considered only when nickel is embrittled by solute hydrogen[2] or in a high fugacity environment[22]. Because intergranular cracks are often found to initiate at free surfaces the high pressure bubble mechanism is for the most part not applicable, and has fallen into disfavor as a nickel hydrogen embrittlement mechanism.

1.2.3 Decohesion/surface adsorption

The decohesion mechanism is based on the theory that solute hydrogen decreases atomic bond strength and consequently promotes brittle cleavage fracture. This mechanism was originally put forth by Troiano and co-workers[23] to explain hydrogen assisted cracking of iron, and has been suggested as a cause of hydrogen embrittlement of nickel by Kamdar[14] and Wilcox et al[2]. Direct evidence to support this mechanism could be obtained if the lattice potential as a function of hydrogen content could be determined; up to this time the determination has not been made for any material.

A mechanism related to decohesion is the effect of hydrogen adsorption on the thermodynamic surface energy. The Griffith criterion, modified to include the energy of plastic deformation associated with fracture of ductile materials, is as follows in the case of plane strain crack propagation

$$\sigma_f = \left[\frac{2E(\gamma_s + \gamma_p)}{\pi a(1-\nu^2)} \right]^{1/2} \tag{1}$$

where E is the elastic modulus, a is the crack length, σ_f is the applied stress necessary to propagate the crack, γ_s is the thermodynamic surface energy and γ_p is a term added to the surface energy to take into account energy dissipated in the form of plastic deformation. If hydrogen adsorbed on the fracture surface reduces γ_s, the crack will propagate at a lower stress. A number of objections may be raised to the surface adsorption embrittlement mechanism, the most obvious being that γ_p in the case of a ductile material such as nickel is very much greater than γ_s, and as a result changes in γ_s will not have a marked effect on fracture stress.

1.2.4 Plastic deformation effects

Several hydrogen embrittlement mechanisms have been proposed based on the effect of hydrogen on plastic deformation. Studies providing evidence for this mechanism can be considered to fall into one of two categories; 1) the effect of hydrogen on deformation process at crack tips (where the surface area to deformation volume is high) and 2) the effect of hydrogen on bulk deformation (where the surface area to deformation volume is low).

In the former category, Beachem[24] proposed a model that is based on the effect of hydrogen on crack tip deformation. Beachem suggested that sufficiently concentrated hydrogen dissolved in the lattice just ahead of the crack tip aids in deformation on a microscopic scale and therefore escapes detection except in the electron microscope.

Direct observations of the effect of hydrogen on crack tip plastic processes has been observed by deforming nickel TEM samples in situ in an environmental cell[25]. The fracture of TEM samples was transgranular, ductile in nature and independent of straining environment (H_2, He or vacuum),

however the introduction of hydrogen gas caused the fracture to advance at lower stress levels than in He or vacuum.

Lynch[26] has studied the hydrogen environment embrittlement and liquid-metal embrittlement in notched nickel single crystals at room temperature. Plastic deformation associated with fracture in mercury and hydrogen environments, although less than that for fracture in argon, was extensive, with large dimple formation on fracture surfaces. The fractures produced in mercury were found to be almost indistinguishable from those produced in hydrogen. Since LME of nickel in liquid mercury can be attributed to the effects of chemisorption, Lynch concluded that the hydrogen embrittlement observed was also due to chemisorption and that hydrogen chemisorption at that crack tip affected dislocation nucleation. In support of this mechanism, a recent study by Wei[27] has shown that the crack growth rate of cold rolled Ni is increased in a hydrogen environment at -196°C. Since hydrogen is essentially immobile in nickel at -196°C, Wei speculated that the increase in crack growth was due to the effect of hydrogen adsorption on dislocation formation processes at the crack tip.

As mentioned previously, solute hydrogen has been shown to affect the degree of planar slip of nickel when dislocation and hydrogen drift velocities are comparable. It has been suggested that the presence of this condition (less homogeneous slip in the bulk) will cause stress concentrations at grain boundaries which in turn will promote intergranular fracture[28]. However this does not provide a viable explanation of the observed embrittlement at -196°C where hydrogen has no effect on bulk deformation.

1.3 Hydrogen Segregation to Grain Boundaries

As previously stated, the fracture mode of hydrogen embrittled nickel is predominantly intergranular. Although the actual mechanism of hydrogen embrittlement is not well established, it can be surmised that the attainment of conditions which lead to embrittlement will depend on lattice transport processes in order that a critical concentration of hydrogen at grain boundaries be attained. Two transport processes are considered to be important and will be considered in the following sections; thermally activated lattice diffusion and transport of hydrogen by mobile dislocations.

1.3.1 Diffusion

The diffusivity of hydrogen in nickel has been shown to have Arrhenius dependence;

$$D_H = D_0 \exp \left[- \frac{Q_0}{kT} \right] \tag{2}$$

over the temperature range 0-1396°C and to be insensitive to grain size (30-120 μm) and dislocation density. Robertson[29] determined best values for D_0 and Q (6.44 ± .35 x 10^{-3} cm^2/sec and 9610 ± 60 cal/mole respectively) by performing hydrogen permeation experiments and reviewing values previously reported in the literature. The following table lists the diffusivity of hydrogen in nickel at temperatures important to this study.

Table 1

Diffusivity of Hydrogen in Nickel

T(°C)	D cm^2/sec
45	1.5×10^{-9}
20	4.1×10^{-10}
-20	3.0×10^{-11}
-65	4.7×10^{-13}
-196	2.7×10^{-30}

Solute hydrogen may segregate to grain boundaries during aging provided that the temperature is sufficiently high to allow diffusion and there is a driving force (the chemical potential of H is higher in the lattice than at or adjacent to the grain boundary). Assuming a negative binding enthalpy of hydrogen to a grain boundary trap, an increasing concentration of trap sites will be filled at equilibrium as the aging temperature is decreased provided they are not saturated. At the same time it is expected that increased time will be required to reach an equilibrium condition as the temperature is lowered since the diffusivity decreases with temperature.

The segregation of hydrogen (deuterium) to surfaces and grain boundaries in nickel has been observed by Fukushima and Birnbaum[7] using secondary ion mass spectroscopy (SIMS) techniques. Nickel specimens were thermal charged in one atmosphere of H_2 gas at 1500°K, quenched into silicone oil and stored at -196°C prior to use. Before aging, a homogeneous distribution of hydrogen was observed. Various aging profiles (Fig. 2) were used to allow diffusion of hydrogen to grain boundaries. The resulting segregation is shown in Fig. 3. The segregation of sulfur to external surfaces and co-segregation effects for sulfur and hydrogen were also examined. In the presence of sulfur at grain boundaries, segregation of hydrogen was shown to exist in the as quenched condition (quenching temperature of 572°C), and upon aging additional hydrogen segregation occurred. This result implies a relatively high binding enthalpy between hydrogen and sulfur.

1.3.2 Dislocation Transport

The concept that hydrogen is transported in the form of Cottrell atmospheres on moving dislocations was first suggested in 1951 by Bastien and Azou[30] as an explanation of the observed strain, strain rate and temperature

15

Figure 2.   Aging profiles used by Fukushima and Birnbaum[7] to study hydrogen
             segregation to boundaries in nickel. SIMS measurements were
             performed at -78°C.

Figure 3.   The hydrogen profile across a grain boundary determined by
             Fukushima and Birnbaum. Specimen was thermally charged with
             hydrogen (~ 500 ppm) and aged to 22°C prior to SIMS analysis.
             Each curve is labeled by the mean sputtered depth during data
             acquisition.
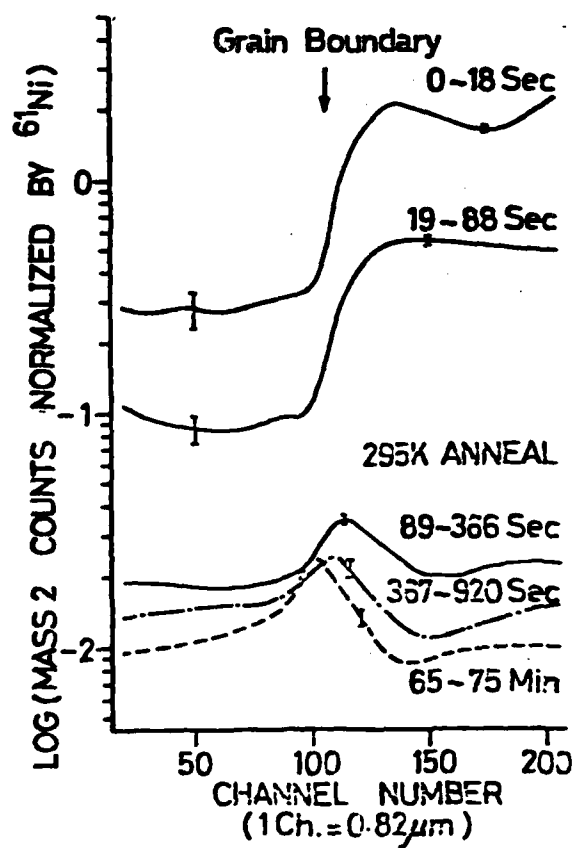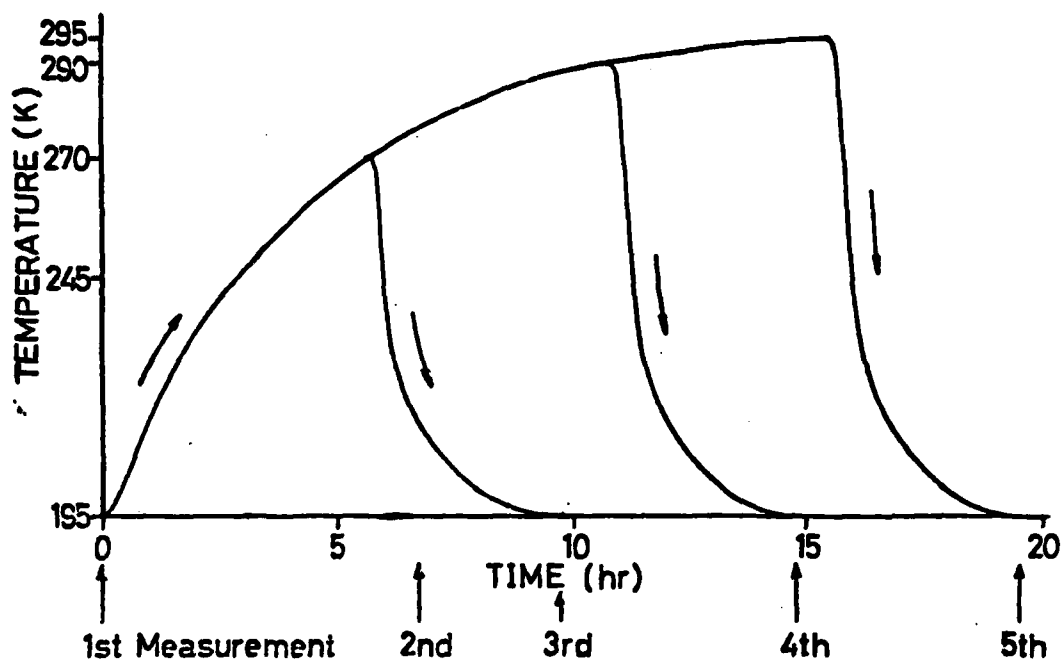
dependence of hydrogen assisted fracture of iron and steel. The enhanced release of hydrogen (tritium) from charged specimens during deformation of nickel[31] provides substantial evidence that dislocation transport can occur at rates considerably faster than that which can occur by lattice diffusion alone.

Several parameters are considered to play a role in the transport of hydrogen by dislocations. In the presence of the internal stress field of a dislocation, the hydrogen concentration about the dislocation is given by,

$$C_\perp = C_0 \exp - [\frac{\Delta H_{Dis}}{kT}] \tag{3}$$

where C_0 is the solute concentration in regions unaffected by the internal stress fields of dislocations, k is the Boltzman constant and ΔH_{Dis} is the binding enthalpy between a hydrogen atom and a dislocation[32]. For the purposes of this study, the value of ΔH_{Dis} given by Boniszewski et al[1] of -0.08 eV is appropriate. At low temperatures considerable enhancement of hydrogen concentration will occur in a dislocation stress field if sufficient time is allowed for segregation to occur (eg. $C_\perp/C_0 = 100$ @ -65°C).

A mobile dislocation will carry its associated hydrogen atmosphere along with it if the velocity of the dislocation does not exceed the drift velocity of hydrogen. The critical velocity, V_c, of a dislocation before it breaks away from its associated Cottrell atmosphere is given by the following relationship[22],

$$V_c = \frac{D_H}{kT} \frac{E_B}{30b} \tag{4}$$

where D_H is the diffusivity in nickel and b is the Burgers vector.

The corresponding critical strain rate for a value of V_c can be obtained using the Orowan expression

$$\dot{\varepsilon}_c = \rho V_c b \tag{5}$$

where ρ is the mobile dislocation density. Combining equations 3, 4 and 5 the critical strain rate can be written as follows:

$$\dot{\varepsilon}_c = \left(\frac{\rho E_B D_o}{30K}\right) \left(\frac{1}{T}\right) \exp\left(\frac{-Q_o}{KT}\right) . \tag{6}$$

If the critical strain rate is exceeded, mobile dislocations will not have an appreciable effect on hydrogen transport. The dislocation density for small strains is estimated to be about 10^8 cm^{-2}[33]. Using this value for ρ and the appropriate values for E_B, D_o, Q_D and k the critical strain rate at -196°C is 10^{-38} sec^{-1}. Thus at this temperature it is expected that no significant concentration of hydrogen will be transported via dislocation motion at any reasonable strain rate, eg. 10^{-5} sec^{-1} or higher.

At -65°C the diffusivity of hydrogen in nickel is much higher than at -196°C, and as a result hydrogen may be swept along with mobile dislocations provided the critical strain rate is not exceeded. The critical strain rate at -65°C is calculated to be about 10^{-4} sec^{-1} using equation 6. To investigate the effect of dislocation transport of hydrogen on the embrittlement of nickel, testing at -65°C can be performed at two strain rates; one higher than the critical strain rate, in which case dislocation transport will not occur, and one slower than the critical strain rate, in which case dislocation transport should occur.

Evidence of dislocation transport of hydrogen in nickel at about this temperature (-80°C) and at a strain rate of $3.3 \times 10^{-4} \text{sec}^{-1}$ has been given in work by Wilcox and Smith[2]. A series of hydrogen charged specimen were strained in tension to various amounts short of fracture (0-18.5% elongation). The gage lengths were then analyzed for hydrogen content. It was found that the hydrogen content decreased linearly with strain with a maximum decrease of 18% occurring at 10% elongation. The acceleration of hydrogen evolution was attributed to hydrogen atmospheres dragged along with dislocations being released when the dislocations emerged at a free surface.

1.4 Embrittlement Due to Sulfur Segregation at Grain Boundaries

Many studies have shown that pure nickel and nickel alloys are embrittled by trace impurities such as sulfur. Lozinskiy et al[34] reported that nickel with a sulfur content of 20 at. ppm exhibits poor ductility as a result of intergranular fracture between about 400 and 950°C. They also reported that if the sulfur content is increased to 40 at. ppm or above, intergranular fracture occurs between room temperature and 950°C. It has been shown that sulfur embrittlement was eliminated by the addition of small amounts of Zr[34] and Mn and Mg[35,36]. The improvement in ductility has in general been attributed to these alloy additions tying up sulfur in the bulk or by sulfide formation. These results indicate that sulfur segregation to grain boundaries is responsible for the observed embrittlement.

Direct observation of sulfur segregation to nickel grain boundaries has been accomplished by Auger electron spectroscopy (AES) of specimens fractured in situ in a high vacuum. Utilizing AES Loier and Boos[10] studied the influence of grain boundary sulfur concentration on the intergranular brittleness of nickel of different purities deformed in tension at -150°C.

They found that the sulfur concentration at grain boundaries in nickel containing globally less than 450 ppm sulfur appeared to be the major factor in the brittleness of the metal.

The temperature dependence of sulfur coverage of Ni surfaces in equilibrium with solute sulfur and H_2S gas has been examined by Miyahara et al[37] using Auger analysis in the temperature range 27 to 1000°C. Their results indicate that saturation coverage occurs at temperatures below about 800°C with the equilibrium coverage decreasing linearly with temperature to a value half of that at saturation at 950°C. It may be assumed that grain boundaries will behave in much the same fashion as a free surface since the enthalpies of segregation are of the same magnitude in many systems.

The effect of grain boundary chemistry on the tensile ductility and fracture mode of nickel at cathodic potentials using a straining electrode technique has been studied by Bruemmer et al[38] and Jones et al[39]. These studies showed that the threshold sulfur composition necessary to induce intergranular fracture is dependent on the hydrogen fugacity which was controlled by the cathodic potential. The observations made were used to suggest that grain boundary impurities (sulfur, hydrogen) contribute to the embrittlement process without altering the mechanism.

Hagiwara and Chene[8] have shown that the embrittlement of hydrogen charged commercial nickel (INCO Ni 200) is sensitive to heat treatments that cause segregation of sulfur at grain boundaries as well as intra and intergranular precipitates when tested at room temperature and to a lesser extent for tests performed at liquid nitrogen temperature. Direct observation of grain boundary hydrogen segregation in undeformed samples was obtained by high resolution tritium autoradiography. It was not determined whether the

sulfur and hydrogen segregation acted synergestically or additively in influencing intergranular failure.

In a study by Sain and Meshii[40] the cosegregation effect of sulfur and hydrogen on grain boundary strength of electrolytically charged iron was studied. It was found that both elements significantly increase the propensity towards grain boundary failure and that the deleterious effects appeared to be additive.

CHAPTER 2

EXPERIMENTAL PROCEDURES

2.1 Specimen Preparation

The study of the effect of hydrogen segregation on grain boundary fracture utilized flat notched tensile specimens which were designated Ni-xx and are shown in Figure 4. The specimen's design was chosen to enhance the ability to obtain fracture mode data; the specimen thickness is relatively small to accommodate fast quenching, and notches allowed for a random sampling of grains and grain boundaries across the relatively large width. In the absence of notches, fracture was initiated at the most susceptible grain boundary and hence the results were biased towards high values of intergranular fracture. All samples used in this study were fabricated from cold rolled, high purity nickel sheet (99.999% nominal purity).

Specimens were given a final anneal prior to charging at 1300°C in nitrogen-5% hydrogen for one hour resulting in an average grain diameter of 0.8 mm which remained unchanged during subsequent thermal charging procedures. Analysis of the specimen material by spark source mass spectrometry and by vacuum fusion analysis subsequent to testing gave the results shown in Table 1.

Experiments performed to determine the effect of strain rate and dislocation transport on fracture behavior utilized dogbone specimens (designated ND-xx and shown in Figure 4) rather than notched specimens, so that the straining rate would be uniform throughout the gage length. ND-xx specimens were machined from the same rolled nickel sheet as were Ni-xx specimens and were given the same thermal treatment prior to charging.

Table 2

Analysis of Impurity Elements
in Nickel Tensile Specimens

Mass Spectrographic Analysis[*]

Element	Concentration (at. ppm)	
	Ni-xx	NSI-xx
Sn	<3	<3
Cu	2	9
Fe	6	7
Mn	0.2	2
Ca	<6	<2
K	4	5
Cl	9	20
S	<4	30
P	unknown	unknown
Si	<7	<20
Al	4	2
Mg	8	4
Na	4	10
Vacuum Fusion Analysis		
S	<1	1
N	1	<1
C	3	21
O	8	4

[*]Mass spectroscopic analysis has an accuracy of +/x a factor of 3.
All elements which are not listed have levels less than 1 ppm.

24

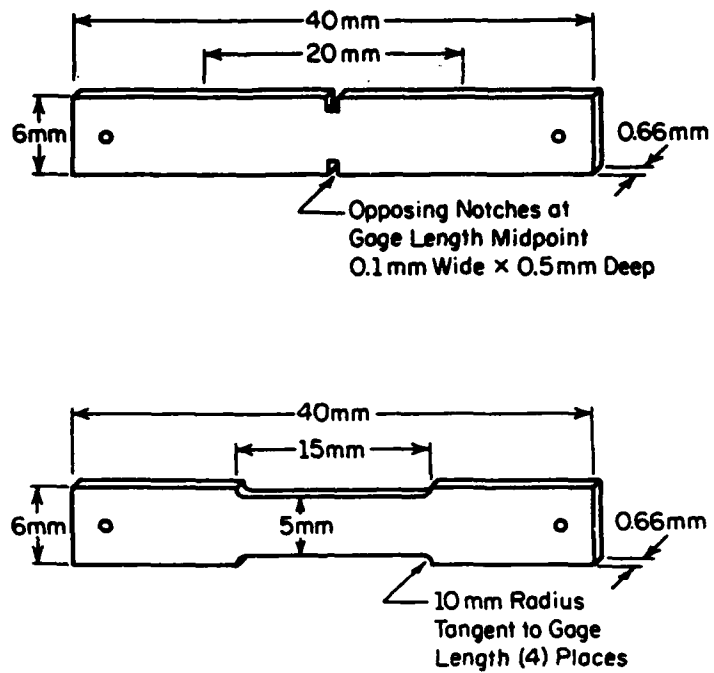

Figure 4.   Ni-xx (NSX-xx) and ND-xx tensile specimens. Samples were
prepared from cold rolled nickel sheet (~ 99.999% Ni).

To investigate cosegregation effects of hydrogen and sulfur on the fracture mode, three batches of notched specimens designated NS1-xx, NS2-xx and NS3-xx were doped with sulfur after annealing at 1300°C in nitrogen-5% hydrogen for one hour. Sulfur was introduced by heating to 850°C in a static H_2S-H_2 atmosphere for 72 hours, followed by slow cooling. This heat treatment was designed to establish a low bulk concentration of sulfur[41] with equilibrium segregation of sulfur at the grain boundaries[13]. The segregation of sulfur at the grain boundaries was verified by in situ fracture and Auger electron spectroscopy of grain boundaries, the details of which are given in Appendix B. A summary of the sulfur coverages at grain boundaries for the three batches of specimens is given in Table 3.

Table 3

Sulfur Coverage of Grain Boundaries in NSX-xx Tensile Specimens

Specimen	P_{H_2S}(Torr)	S/Ni coverage	Depth of Coverage (Å)
NS1	3×10^{-4}	0.06	~ 5 Å
NS2	5×10^{-4}	0.06	~ 50 Å
NS3	5×10^{-5}	0.0	0

2.2 Hydrogen Charging and Aging

Hydrogen was introduced into the specimens Ni-xx and ND-xx by heating to 1150°C for approximately 3 minutes in a static hydrogen-argon atmosphere followed by a rapid quench into water at room temperature. A schematic of the furnace built expressly for the purposes of this work by the author is shown in Figure 5. NSX-xx specimens were charged with hydrogen in the same manner by
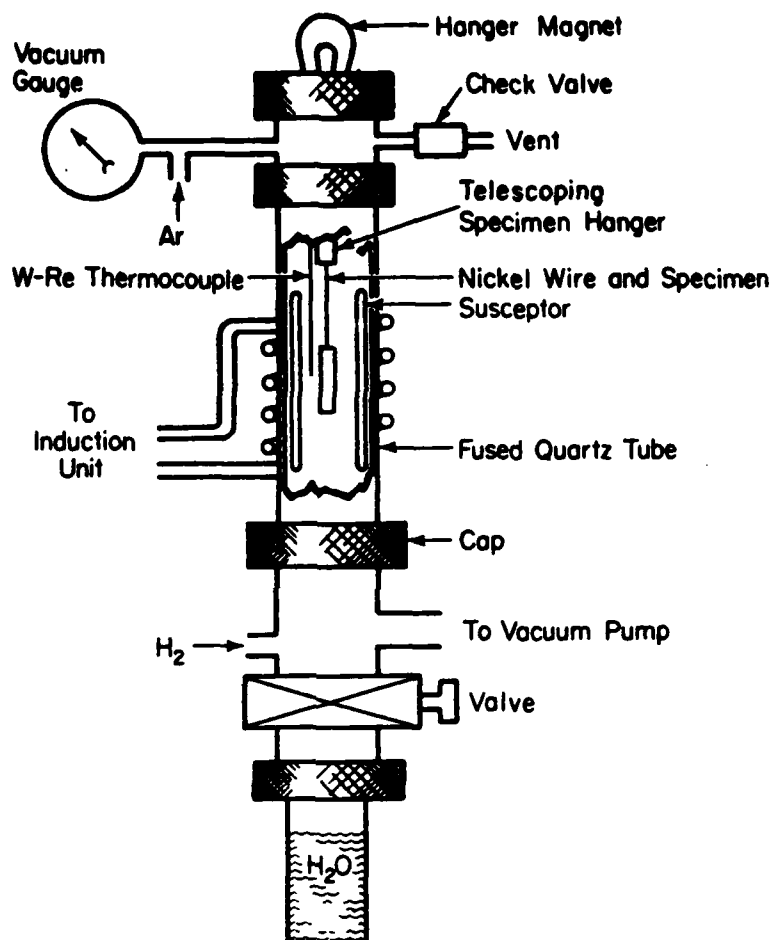
Figure 5.   Schematic of furnace used to thermally charge nickel tensile
specimens. Samples were heated by a molybdenum susceptor which
was coupled to an induction unit.

heating to 850°C for about 3 minutes and then quenching into water. Some NSX-xx samples were held in a vacuum of 10^{-3} torr at 850°C to remove trace amounts of solute hydrogen and were then quenched into silicone oil. The purpose of heating NSX-xx specimens to only 850°C as opposed to 1150°C was to avoid disturbing the equilibrium sulfur distributions at grain boundaries obtained by doping at 850°C.

The desired solute hydrogen content was obtained by adjusting the partial pressure of hydrogen in the furnace between 1.0 and 0.0 (atm.) prior to heating. The resulting solute hydrogen concentration of the charged nickel was calculated using Sieverts law and the solubility data of Robertson[29], which can be combined to yield the following equation;

$$C_H = \sqrt{P_H}\, C_o\, \exp \frac{-\Delta H_s}{RT}$$

where C_H is the bulk hydrogen concentration in cm^3 (NPT) of H_2/cm^3 of nickel, P_H is hydrogen pressure in atmospheres, T is the charging temperature in degrees Kelvin, ΔH_s is the heat of solution (3700 cal/mole), C_o is a pre-exponential (5.72 $cm^3 H_2/cm^3 Ni$) and R is the gas constant.

After quenching into water (or oil), specimens were held at ambient temperature for about 30 seconds before quenching and subsequent storage in liquid nitrogen. This allowed the furnace atmosphere to be exchanged with an inert gas. Aging was carried out in methanol baths at 45°C, -20°C and -65°C after which specimens were again stored in liquid nitrogen prior to testing. Aging times varied between 10 seconds and 260,000 seconds.

2.3 Mechanical Testing

Testing of Ni-xx and NSX-xx specimens was performed at -196°C in a liquid nitrogen bath. This test media was chosen because hydrogen is essentially immobile at liquid nitrogen temperature, consequently solute hydrogen distributions obtained by aging will remain unchanged during testing. Prior to testing, specimens were mounted in a tensile stage immersed in liquid nitrogen and were exposed to somewhat elevated temperatures for only brief moments while being transferred from one nitrogen bath to the next. This procedure was followed to avoid alteration of the distribution of hydrogen due to aging procedures. Testing was performed at a nominal strain rate of 3.3×10^{-4} sec^{-1} utilizing an Instron machine modified to facilitate testing in liquid nitrogen, as shown in Figure 6.

Testing of ND-xx specimens was performed in a dry ice methanol bath, the temperature of which was found to be -65°C. In the testing of ND-xx specimens two strain rates were employed, 3×10^{-2} sec^{-1} and 3×10^{-5} sec^{-1}. The critical strain rate with respect to dislocation transport of hydrogen at -65°C was calculated to be about 10^{-4} sec^{-1} for a mobile dislocation density of 10^8 cm^{-2}. Thus, at the slow strain rate dislocation sweeping of hydrogen should occur and at the faster strain rate it should not. To account for the difference in aging time that occurs during testing due to the difference in strain rate (60 seconds at 3×10^{-2} sec^{-1} vs. 7.2×10^3 seconds at 3×10^{-5} sec^{-1}), a series of specimens were aged at the test temperature for 7.2×10^3 seconds prior to testing at a strain rate of 3×10^{-2} sec^{-1}.
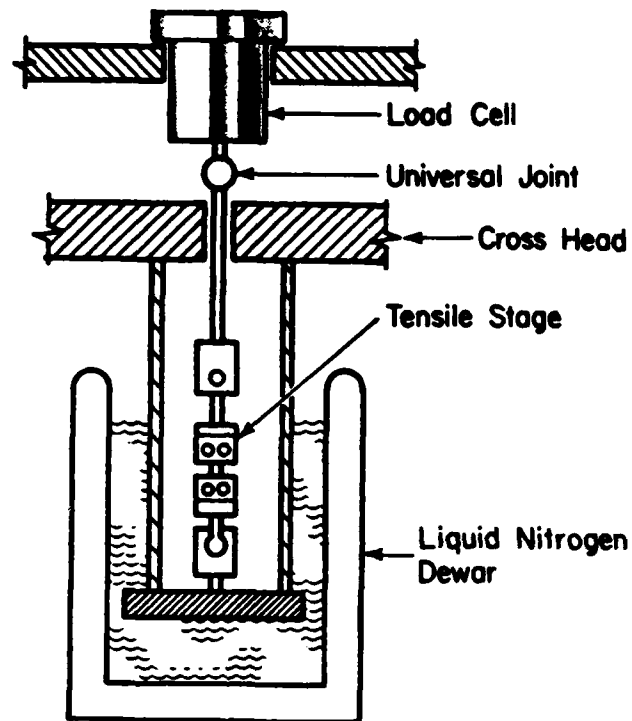
Figure 6.   Schematic of the tensile testing set up for testing samples in liquid nitrogen or methanol-dry ice baths. The tensile stage hung free until loading.

CHAPTER 3

RESULTS

The results of tensile tests performed to evaluate the effects of diffusive hydrogen segregation, dislocation transport of hydrogen and co-segregation of sulfur and hydrogen on fracture mode are given in this chapter. The fracture modes were found to be either ductile shear rupture, intergranular, or some combination of these modes. The percentage of intergranular fracture was used to gage the degree of embrittlement of each specimen. To determine the percent of intergranular fracture SEM photographs (18X magnification) were taken of all fracture surfaces. A linear intercept method was then used in conjunction with the SEM photographs to calculate the percent intergranular fracture of each specimen. Detailed fractography of fracture surfaces is presented in section 3.5. A listing of test specimens and pertinent data (T_{age}, t_{age}, C_H, etc.) is given in Appendix A.

3.1 Hydrogen Segregation to Grain Boundaries

The results of tensile tests performed in liquid nitrogen to determine the effect of hydrogen segregation on fracture mode are presented in this section. The fundamental results are plotted in the form of percent intergranular fracture vs. aging time or bulk hydrogen concentration. The former was used to evaluate the kinetics of embrittlement and the latter to investigate the thermodynamics of hydrogen trapping at grain boundaries, both of which will be analyzed in the following chapter.

3.1.1 Dependence of Intergranular Fracture on Aging Time

Tests were performed to investigate the effect of aging time on the fracture mode. This was accomplished by holding the aging temperature and bulk hydrogen concentration constant for a given set of specimens while varying the aging time, thus allowing varying amounts of hydrogen to accumulate at grain boundary trapping sites. Due to the high hydrogen supersaturation, loss of hydrogen due to outgassing during aging is inevitable although only a small percentage is lost. Thus true equilibrium with respect to hydrogen segregation at grain boundaries cannot be realized. Because of this, the condition at which intergranular fracture appears to be a maximum will be referred to as "quasi equilibrium". The aging time at which the maximum embrittlement condition prevails is denoted "the critical aging time", t_c.

Figure 7 shows the effect of aging specimens containing 765 ppm of hydrogen at 45°C between 10 seconds and 2.6×10^5 seconds. As the aging time increases, the degree of I.G. fracture increases from about 30% at 10 seconds to 70% between 200 and 10^4 seconds and upon further aging the propensity for intergranular fracture decreases. The decrease in grain boundary fracture for aging periods exceeding 10^4 seconds is most likely due to decreases in bulk hydrogen concentration from outgasing, which results in a decreasing hydrogen concentration at grain boundaries.

Figure 8 shows the results of aging samples containing 275 ppm, 440 ppm and 660 ppm of hydrogen at -20°C between 10 seconds and 2.4×10^5 seconds. Specimens containing an insufficient amount of hydrogen to promote 100% IG fracture reach what appears to be intergranular fracture maxima at about 10^4 seconds. The results of aging specimens containing 95 ppm and 45 ppm hydrogen
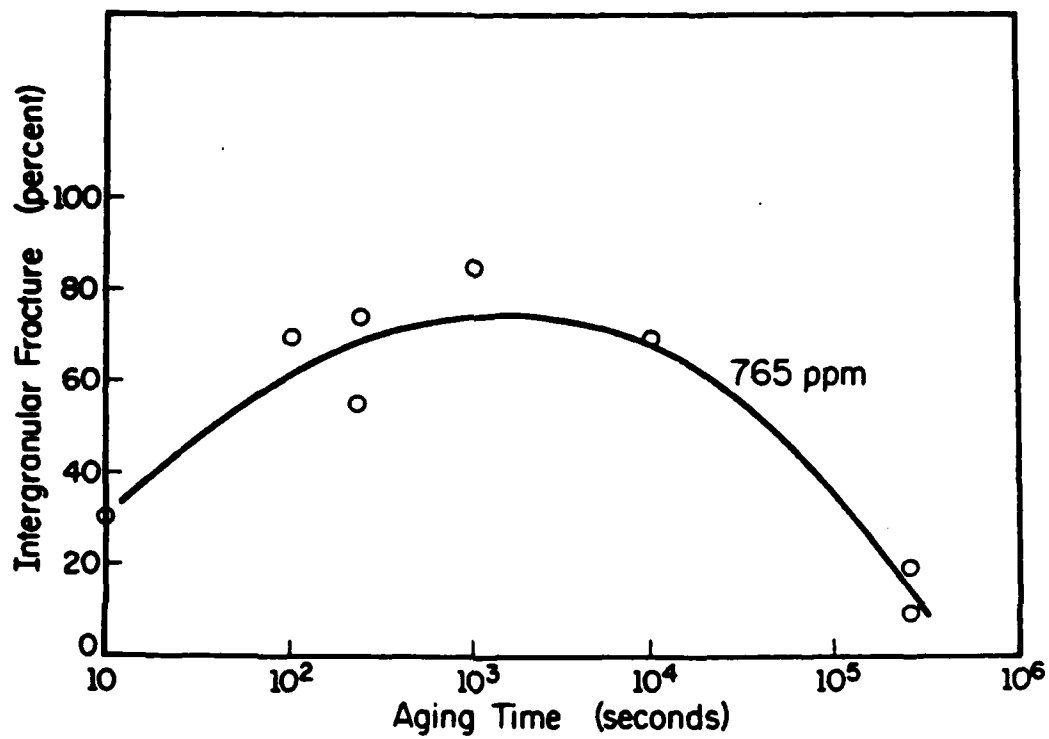
Figure 7.   Variation of percent intergranular fracture with aging time at
            45°C. Specimens reverted to ductile behavior after a large
            percentage of the bulk hydrogen concentration was lost due to out-
            gassing. The critical aging time is about 240 seconds.
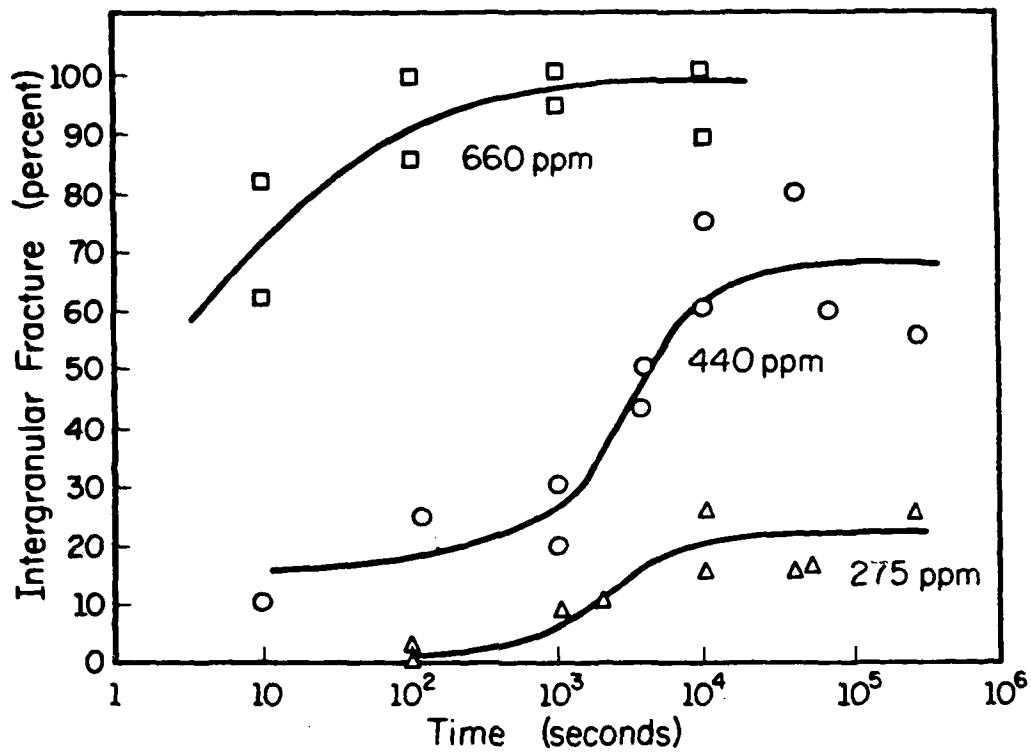
Figure 8.   The effect of aging time at -20°C on percent intergranular
            fracture for specimen containing various levels of bulk hydrogen
            concentration. The critical aging time at this aging temperature
            is 10^4 seconds.
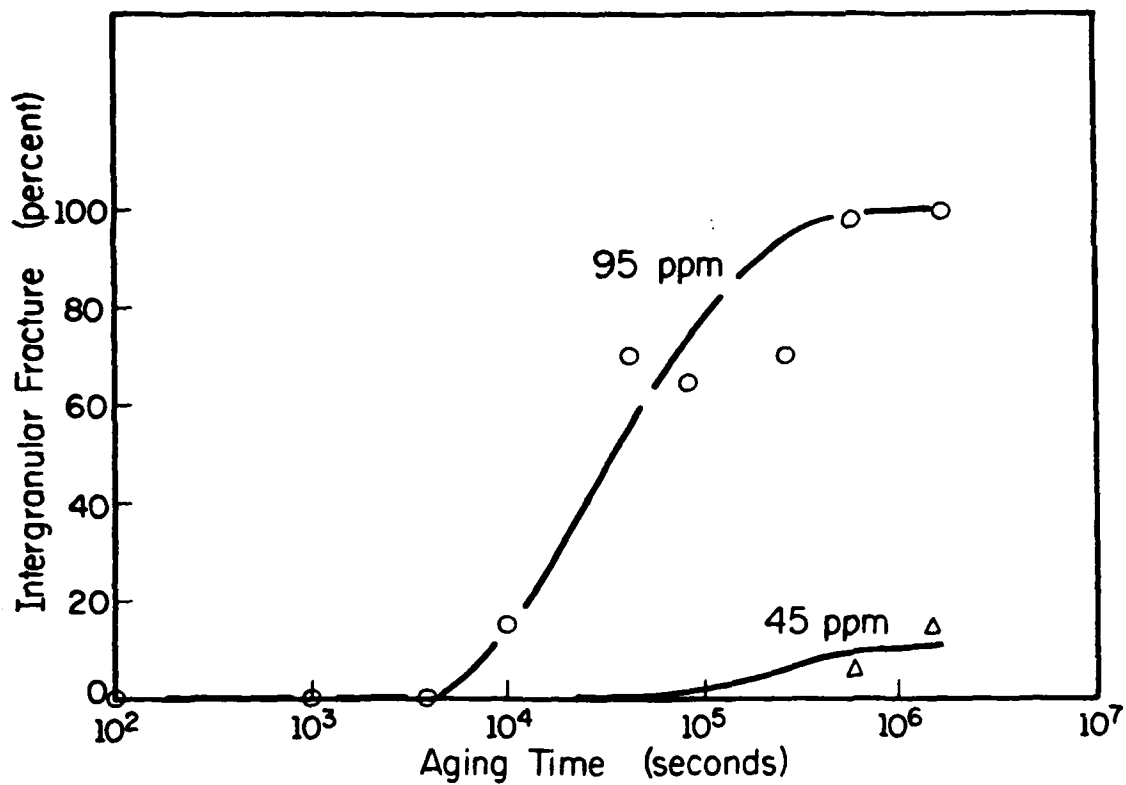
Figure 9.   Variation of intergranular fracture with aging time at -65°C.
The critical aging time is 6×10^5 seconds.

at -65°C are given in Figure 9. The 95 ppm curve rises from 0% IG fracture at 4×10^3 seconds to a value of IG fracture near 100% at 6×10^5 seconds.

The obvious indication of the data presented in this section is that as the aging temperature is decreased, longer aging periods are required to reach maximum values of intergranular fracture. From the data presented, quasi-equilibrium conditions with respect to IG fracture (in essence grain boundary hydrogen segregation) occur at 200 seconds, 10^4 seconds and 6×10^5 seconds for aging temperatures 45°C, -20°C and -65°C respectively. These values of aging time are shown plotted as a function of reciprocal aging temperature in Figure 10 and will be utilized to analyze the kinetics of hydrogen segregation in section 4.2.

3.1.2 Fracture Mode Dependence on Bulk Hydrogen Concentration

Data were obtained to reveal the effect of aging temperature and bulk hydrogen concentration on fracture mode of specimens aged to attain the maximum amount of intergranular fracture; i.e. specimens aged to attain quasi-equilibrium with respect to grain boundary segregation of hydrogen. A plot of percent intergranular fracture vs. bulk hydrogen concentration is presented in Figure 11. Solid points in Figure 11 represent the maximum values of inter-granular fracture taken from Figures 7 through 9. For instance the value of 70% intergranular fracture was taken from Figure 8 and plotted at the 440 ppm point as part of the -20°C aging temperature curve. The aging times used to generate data depicted as open points in Figure 11 were 240 seconds, 8×10^4 seconds and 6×10^5 seconds for aging temperatures 45°C, -20°C and -65°C respectively. The determination of the binding enthalpy of hydrogen to grain boundary traps based on these data is given in Chapter 4.
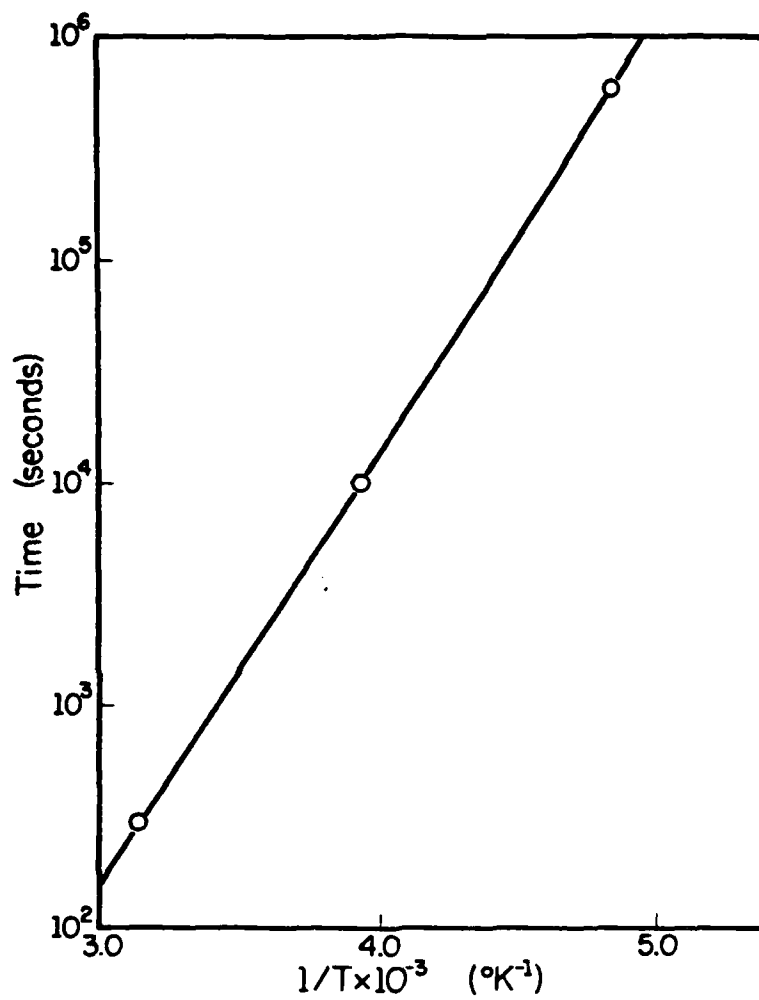
Figure 10.   Critical aging times plotted vs. 1/T (°K⁻¹).

Figure 11. Intergranular fracture vs. bulk hydrogen concentration. Open symbols denote specimens that were aged for periods of time equaling t_c. Solid symbols are levels of intergranular fracture taken from Figures 7, 8 and 9.
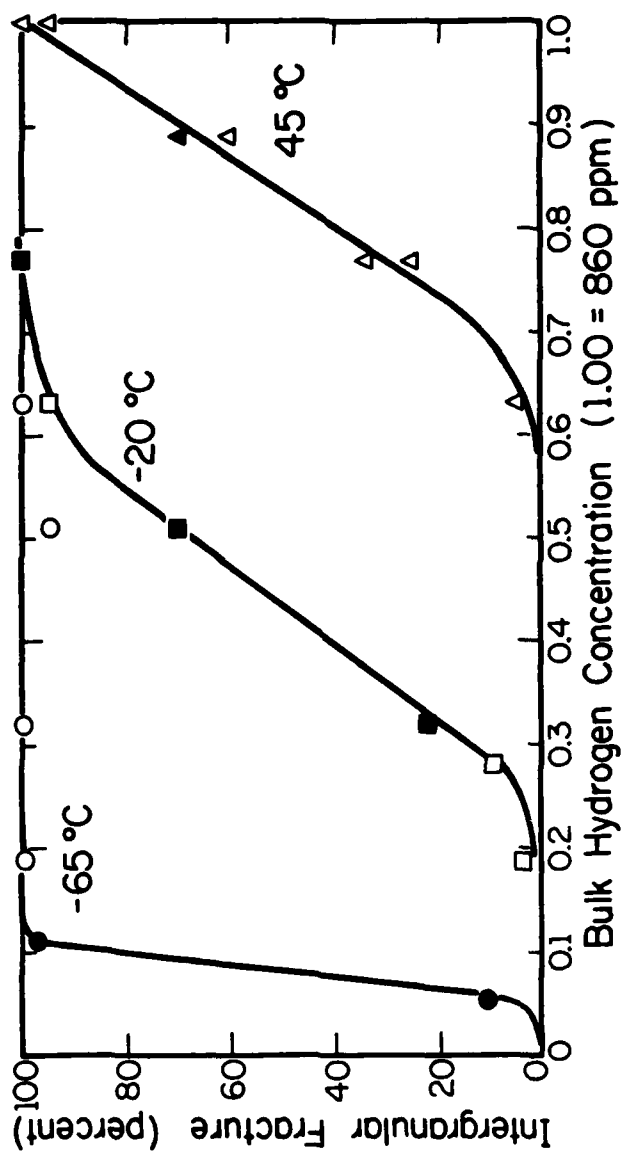
MP-814

3.2 Dislocation Transport

The results of straining nickel dogbone specimens (ND-xx) to failure at -65°C at two strain rates, one faster and one slower than the critical strain rate for hydrogen transport, are given in this section. In some cases specimens were aged at -65°C for a period of time prior to testing.

3.2.1 Effect of Test Temperature on Fracture

Three tensile tests were performed on specimens with 95 ppm hydrogen to determine the effect of testing at -65°C as opposed to -196°C on fracture behavior. The results are shown in Figure 12 along with the results of testing at -196°C subsequent to aging at -65°C previously presented in Figure 9. The data plotted as a function of aging time includes both the period of aging incurred prior to testing and that which occurred during testing at -65°C. The results of these tests indicate an insignificant change in fracture behavior in terms of percent intergranular fracture for the two test temperatures.

Specimens ND-2 and 3 depicted in Figure 12 were aged to a quasi-equilibrium condition at -65°C and were then tested at strain rates of 3×10^{-2} sec^{-1} and 3×10^{-5} sec^{-1} respectively at -65°C. Both samples failed in a predominantly intergranular mode with a relatively insignificant difference in the measured intergranular fracture percent. This result suggests that the strain rate has little effect on fracture behavior, a point that will be explored in the next section.

3.2.2 Effect of Strain Rate

Tests were performed to investigate the effect of strain rate and aging (diffusive segregation) which occurs during testing at -65°C on fracture mode. Results of this study are given in Figure 13 in the form of percent
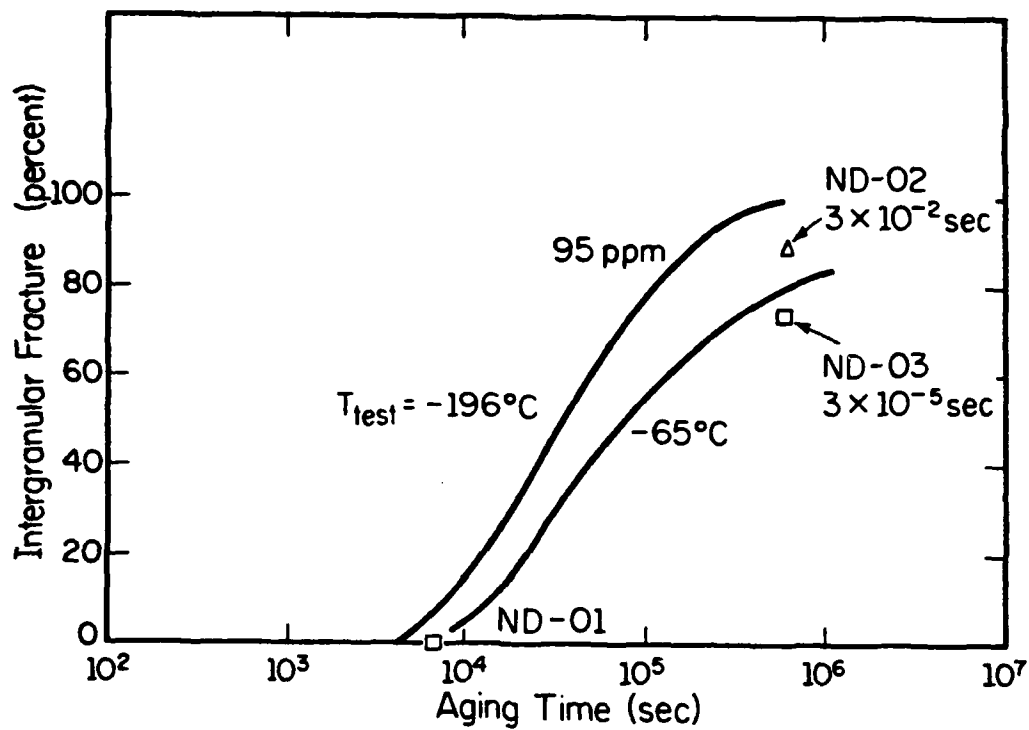
Figure 12. Comparison of the fracture behavior of samples tested at -65°C
with those tested at -196°C. All samples had 95 ppm hydrogen and
were aged at -65°C.
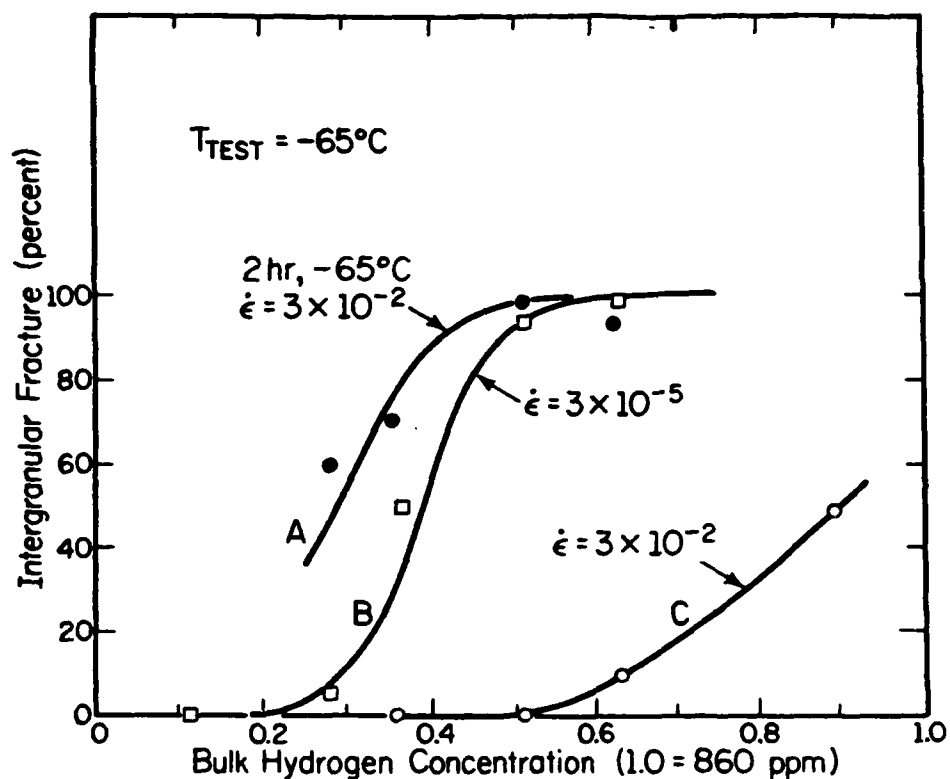
Figure 13. Effect of bulk hydrogen concentration on the percent
intergranular fracture of samples tested at -65 C at
strain rates of either 3×10^{-2} or 3×10^{-5} sec.$^{-1}$.
Solid symbols represent samples aged for 7.2×10^{3}
seconds prior to testing at a strain rate of 3×10^{-2} sec.$^{-1}$.

intergranular fracture vs. bulk hydrogen concentration. The lower curve (C),generated by testing at a strain rate of 3×10^{-2} sec^{-1}, represents a total time of about 250 seconds that the test sample was at -65°C during testing procedures, i.e. an aging time of about 250 seconds which occurred during straining. The middle curve (B) generated by testing at a strain rate of 3×10^{-5} sec^{-1} has significantly more intergranular fracture than curve C. It represents an average total aging time at -65°C of about 7.2×10^3 seconds, the majority of which occurred during testing.

The difference in extent of intergranular fracture between curves B and C for equal hydrogen concentrations cannot be interpreted as due to dislocation transport of hydrogen to the grain boundaries at the slower strain rate as suggested by previous studies. This is shown by the upper curve in Figure 13 (curve A) which was generated by aging specimens for 7.2×10^3 seconds prior to testing at a strain rate of 3×10^{-2} sec^{-1} to account for aging that occurs during the slow strain rate. The data obtained by testing at a strain rate of 3×10^2 sec^{-1} after aging agree with the data generated at the strain rate of 3×10^{-5} sec^{-1} (i.e. curve A equals curve B). This result indicates that the principal variable upon testing at -65°C is the aging time, not strain rate. This strongly suggests that dislocation transport of hydrogen is not a major contributor to the embrittlement of hydrogen charged nickel since the transport of hydrogen by mobile dislocations is expected to be at a maximum at about this temperature.

3.3 Co-Segregation of Hydrogen and Sulfur

Three series of notched specimens NS1-xx, NS2-xx and NS3-xx were doped with sulfur to investigate the effect of co-segregation of hydrogen and sulfur on fracture. Table 3 (Chapter 2) summarizes the coverage, θ, and depth of

coverage, d, of sulfur at the grain boundaries as determined by AES in situ fracture and depth profiling, the details of which are given in Appendix B. Specimens from each series were charged with hydrogen and aged at -20°C for 1.26×10^4 seconds. Figure 14 shows the effect of bulk hydrogen concentration on fracture mode of these specimens when tested in liquid nitrogen. The solid symbols in Figure 14 represent specimens that were heated in a vacuum of 10^{-3} torr prior to quenching into silicon oil at room temperature. The purpose of this treatment was to eliminate hydrogen in solution.

Samples from batch NS1 (about 0.06 monolayer of sulfur at grain boundaries) exibited predominantly intergranular fracture with bulk hydrogen concentrations of 60 ppm or greater. Intergranular fracture decreased to a value of 25% with a sample that had been quenched into water from a wet argon atmosphere. Quenching into oil from a vacuum resulted in completely ductile behavior. This result suggests that the specimens heated in a wet argon atmosphere had retained some hydrogen since a partial monolayer of sulfur was not in itself cause for intergranular fracture. Samples from batch NS2, which had the most sulfur segregation at grain boundaries, failed exclusively in an intergranular mode independent of bulk hydrogen concentration. The fracture behavior of samples from batch NS3 were found to be much like the sulfur free samples, Ni-xx, that were aged to a quasi-equilibrium condition at -20°C, i.e. a given bulk hydrogen concentration results in about the same percentage of intergranular fracture. This result supports the Auger analysis conclusion that the grain boundaries of the NS3-xx specimens are essentially free of sulfur.

Nine specimens from batch NS1 were charged with between 30 and 600 ppm hydrogen prior to aging at 45°C for a period of 300 seconds. The resulting percent intergranular fracture vs. bulk hydrogen concentration is shown in

Figure 14. Intergranular fracture vs. bulk hydrogen concentration for specimen doped with sulfur. All specimens were aged at $-20°C$ for 1.3×10^4 seconds.

Intergranular Fracture (percent) vs Bulk Hydrogen Concentration (1.0 = 600 ppm)

$T_{AGE} = -20°C$
$t_{AGE} = 3\ 1/2\ H$

NS1 (Monolayer)

NS2

NS3
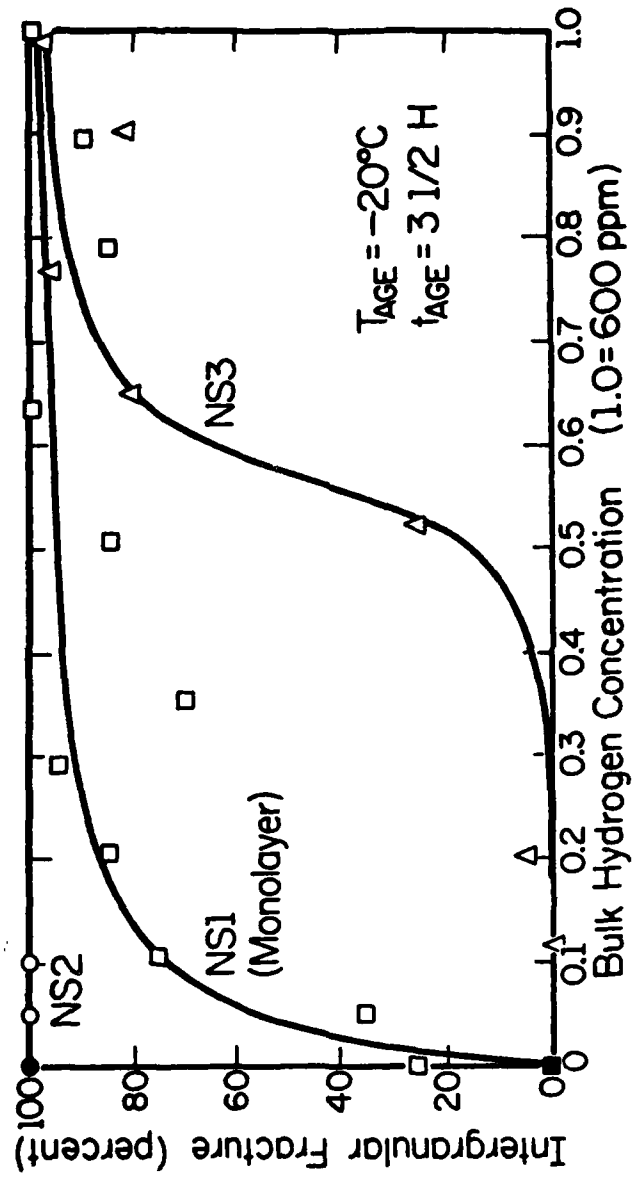
Figure 15. No discernable trend in the data can be ascertained. However, if the data represent a great degree of scatter, which is uncharacteristic of all other sets of data, the intergranular fracture of these specimens is relatively insensitive to bulk hydrogen concentration. No explanation for this behavior can be given at this time.

3.4 Mechanical Properties

It is well documented that the cause of embrittlement of hydrogen charged nickel is due to the intervention of grain boundary fracture which gives rise to substantial reduction of macroscopic ductility (percent elongation, percent reduction of area) and fracture stress. The nature of the samples used in this study are not well suited to the attainment of quantitive mechanical properties such as these due to the geometry and large grain size. Never-the less it is useful, in a qualitative sense, to show the correlation between percent intergranular fracture, elongation and fracture stress.

3.4.1 Stress-Strain Behavior

Within the resolution of the stress-strain data taken during testing there was no effect of hydrogen on the yield strength or work hardening rate of nickel. The typical stress-strain behavior of a hydrogen free or charged but unembrittled Ni-xx tensile bar tested in liquid nitrogen at -196°C at a strain rate of 3×10^{-4} sec^{-1} is given in Figure 16. The yield strength under these test conditions is about 40 Mpa. The elongation and fracture strength at the point of plastic instability (e.g. when necking occurs) of umembrittled specimens was about 40 percent and 49 MPa respectively.

Figure 15. Variation of intergranular fracture NS1-xx samples with bulk hydrogen concentration. Specimens were aged at 45°C for 300 seconds prior to testing in liquid nitrogen.

48
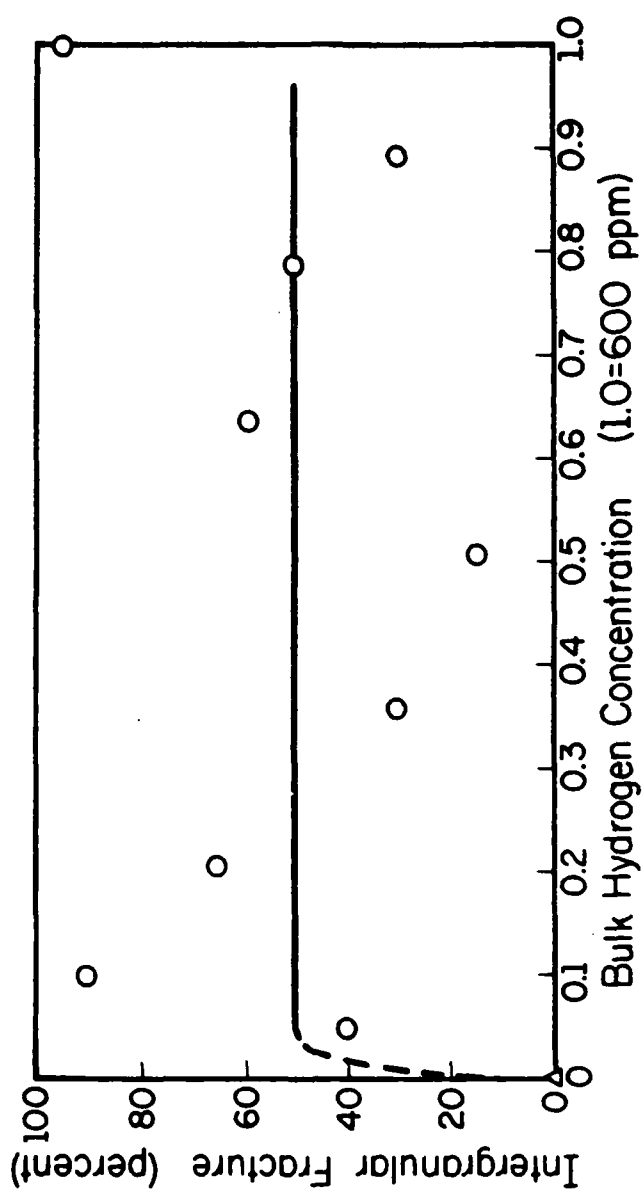
The effect of hydrogen charging and aging is to promote intergranular fracture which causes in essence premature failure. The dotted line in Figure 16 illustrates the stress-strain behavior of a severely embrittled sample (~ 75% intergranular fracture) from the point of crack initiation to specimen separation. The non-monotonic stress-strain behavior of the fracture process is due for the most part to plastic processes which occurred during transgranular shear rupture occurring along approximately 25 percent of the fracture path. This stress strain behavior during crack growth may also be due in part to plastic processes which occur during intergranular fracture as has been documented by in situ SEM fracture studies by Heubaum[6].

3.4.2 Percent Elongation

In Figure 17 percent elongation is plotted vs. aging time for specimens with 95 ppm hydrogen in solution that had been aged at -65°C and tested in liquid nitrogen. This figure can be compared to Figure 9 which shows the effect of aging time on percent intergranular fracture. As one would expect the elongation drops off sharply at about the same aging time (~ 10^5 seconds) that the percent intergranular fracture increases from zero. The elongation at aging times less than 10^4 seconds is essentially that of hydrogen free samples.

Figure 18 depicts the effect of bulk hydrogen concentration on percent elongation for specimens aged to quasi-equilibrium conditions at 45°C, -20°C and -65°C. This figure can be compared to Figure 11 which shows the effect of the same parameters on percent intergranular fracture. As was in the previous example, change in percent elongation can be correlated with percent intergranular fracture for a given bulk hydrogen concentration.

50

Figure 16. Typical stress-strain behavior of an embrittled and unembrittled Ni-xx specimen. Note the discontinuous stress-strain behavior of the embrittled specimen indicating relatively slow crack growth for a "brittle" fracture.

Unembrittled specimen

Embrittled Specimen

Strain (percent) $(\frac{\Delta \ell}{\ell} \times 100)$

Stress (MPa) $(\frac{P}{A_0})$

500 400 300 200 100 0

0 5 10 15 20 25 30 35 40 45
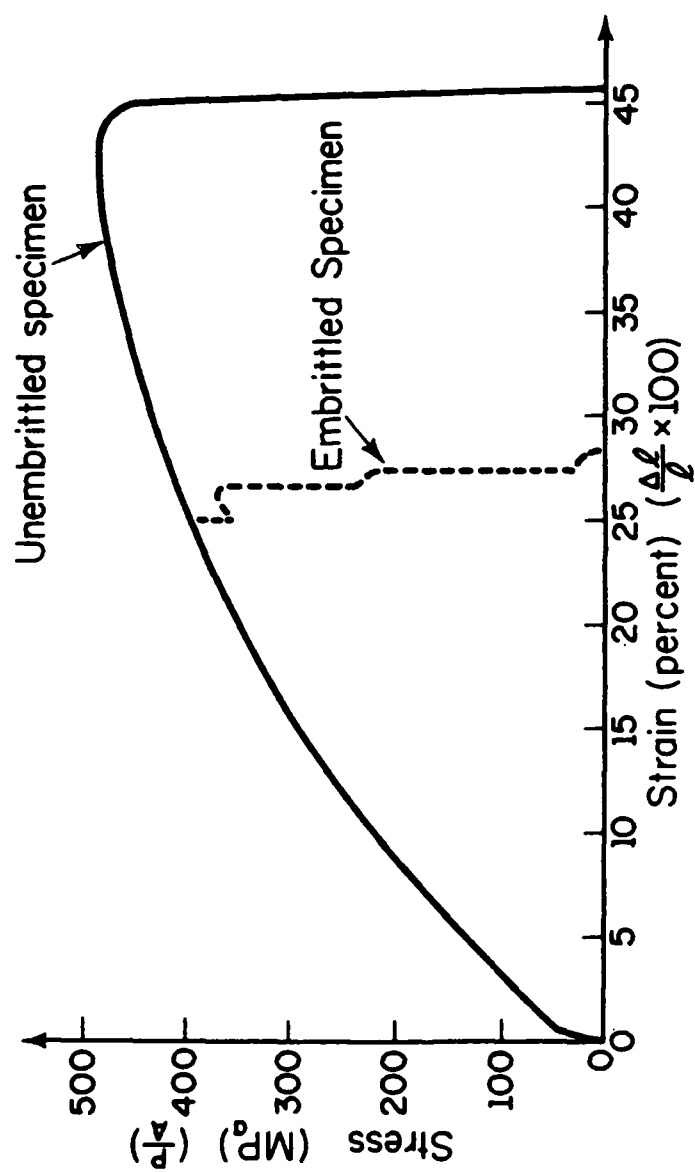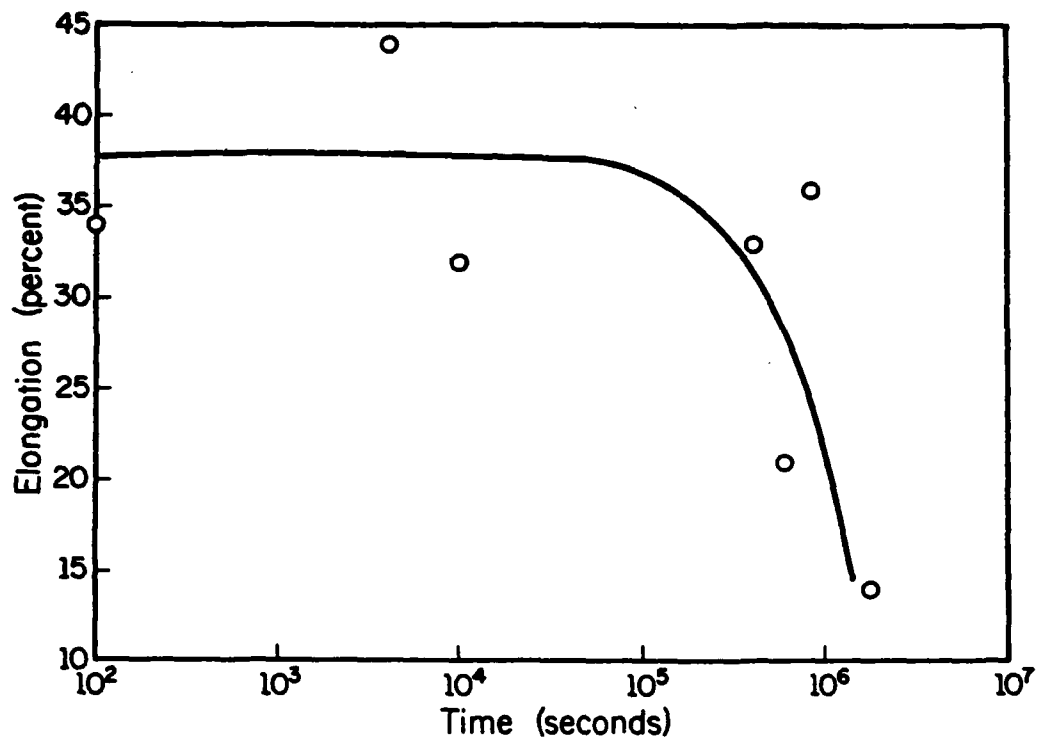
Figure 17. Variation of elongation of Ni-xx specimens with aging time at
-65°C. The data show a strong correlation with that presented in
Figure 9.

3.4.3 Fracture Strength

As one would expect, fracture strength shows the same correlation with intergranular fracture as did percent elongation. Figure 19 shows the effect of aging time at -65°C on the fracture strength of Ni-xx specimens with 95 ppm hydrogen. The fracture strength is shown to drop sharply at about 10^5 seconds as did the percent elongation.

3.5 Fractography

From a macroscopic point of view all fracture surfaces of specimens tested in this study were found to be comprised of either intergranular or ductile shear rupture areas or a combination of these as illustrated in Figures 20-22. To investigate fracture surfaces with a higher resolution, a high resolution scanning electron microscope (ISI model) was used. Because nickel is ferromagnetic and affects the focusing of the electromagnetic objective lens, resolution was limited to about 0.2 μm.

After a careful study of many fracture surfaces it was found that fracture surface features were common to all specimens, i.e. intergranular fracture morphology was independent of aging temperature, duration of aging time and test temperature. An exception to this observation is the NS2-xx specimens which were found to have a more brittle or featureless fracture surface due presumably to the presence of a relatively large amount of sulfur at the grain boundaries.

Fractographs of a typical shear rupture fracture are shown in Figures 23 and 24. Prominent features are the great degree of necking that accompanies fracture and the elongated dimples opposite a smooth sheared region.

54

Figure 18. Elongation vs. bulk hydrogen concentration of samples aged to quasi-equilibrium conditions at -65°C, -20°C and 45°C.

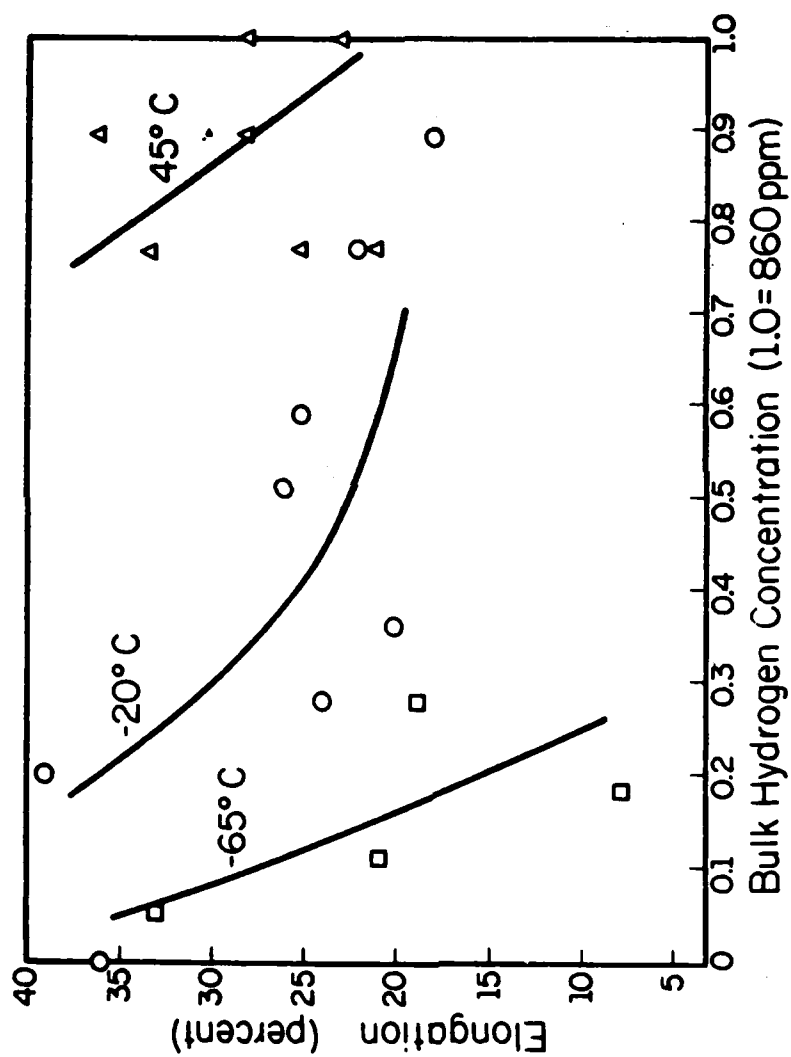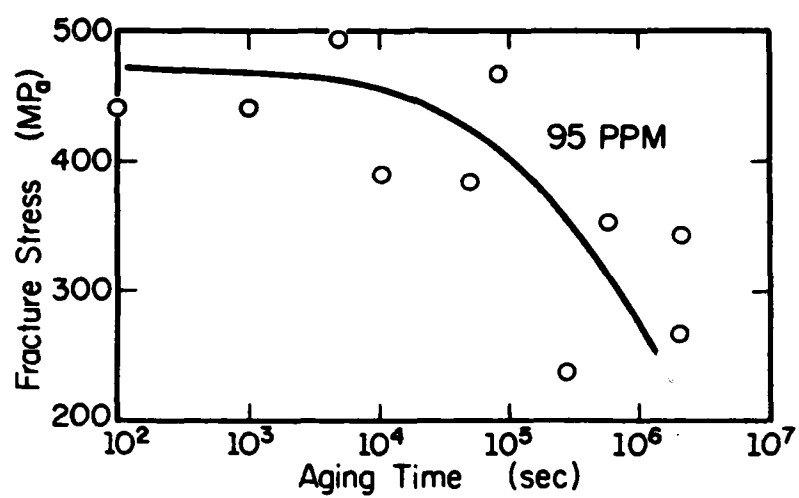Figure 19.   Fracture stress vs. aging time at -65°C for specimens containing
              95 ppm hydrogen.

Figures 25 and 26 illustrate typical intergranular fracture surfaces. The features observed on different grain boundaries varied considerably. In some cases slip lines on the fracture surface were coarse, straight and well defined; in other cases the fracture surface slip lines were found to be closely spaced and wavy indicating much cross slip had occurred within the particular grain. These features are illustrated in Figures 27 and 28. A fractograph of a NS2-xx grain boundary fracture is shown in Figure 29 which is typical of fracture surfaces observed on specimens of this batch. In comparison to other intergranular fractures the NS2-xx specimens with the greatest amount of sulfur at the grain boundaries were found to have a brittle appearance with sharp well defined slip lines.

Small holes approximately 0.5 to 1.5 μm in diameter appeared on most grain boundary fracture surfaces as shown in Figure 30. The spacing and density of these holes varied a great deal and in some cases bands of holes were observed. Large holes were found to have matching holes on matching fracture surfaces, thus the holes were apparently spherical voids prior to fracture.

To investigate the origin of these holes transmission electron microscopy was performed on samples before testing. Thin foils were prepared by thinning material electrolytically at 5 volts in a 80% methonal 20% nitric acid solution at room temperature to a thickness of about 0.05 mm. Disks punched from the thinned material were then prepared by a commercial jet polishing unit using an 80% methanol 20% H_2SO_4 solution at -20°C. Voids were observed in samples prepared from material that had been hydrogen charged (860 ppm) and aged to or beyond quasi-equilibrium at the three aging temperatures used in

this study as well as from material that had only been annealed at 1300°C in N_2-5% H_2 for one hour. Representative micrographs are shown in Figures 31 and 32. Because voids were present in the material before hydrogen charging and aging it is assumed that the bubbles were a result of a reaction between interstitial c. n and/or oxygen present in the as received condition of the material and hydrogen which occurred during annealing at 1300°C in N_2-5% H_2 gas.

Because of the supersaturated condition of the material after charging, the possibility exists that hydrogen precipitation in voids during aging could have caused void growth. Void growth of this nature has been observed in hydrogen charged and aged copper by Wampler et al.[42]. TEM observations revealed an appreciable dislocation density associated with the voids in addition to prismatic loops presumably punched out during void growth. None of these indications of void growth were observed in TEM foils prepared from the hydrogen charged and aged nickel used in the current study.

It is not expected that the voids observed on fracture surfaces and in the bulk had a marked effect on the results of this study for two reasons; 1) the lack of evidence of void growth due to aging and 2) the void density had no effect on fracture surface morphology i.e. the fracture surfaces looked the same whether or not voids were present.

Figure 20. SEM fractograph of specimen Ni-70 showing a typical example of complete ductile rupture type failure. Specimen had 540 ppm solute hydrogen and was aged at 45°C for 240 seconds prior to testing in liquid nitrogen at a strain rate of 3.3×10^{-4} sec^{-1}.

Figure 21. Fractograph of specimen Ni-51. This specimen had the same hydrogen content as the one shown in Figure 20, but was aged at -65°C for 6×10^5 seconds prior to testing which resulted in 100% intergranular fracture.

Figure 22. Fracture surface of specimen Ni-10 showing a mixed mode failure. About 60% of the fracture is intergranular, 40% ductile rupture. This specimen had 440 ppm solute hydrogen and was aged at -20°C for 8.6×10^4 seconds.
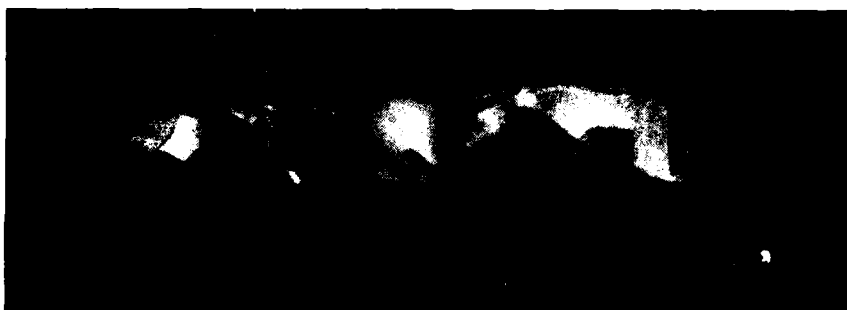
1 mm

Figure 23.   SEM fractograph of a ductile shear rupture failure. Specimen
was fractured in liquid nitrogen at a strain rate of 3.3×10^{-4}
sec^{-1}. Note the considerable amount of necking that accompanies
this fracture mode.

Figure 24.   High magnification micrograph of the fracture surface shown in
Figure 23. The elongated dimples indicate internal microvoid
formation prior to specimen separation in a ductile shear mode.

10KV   359X   50U 0004

10KU   2 69KX   10U 0006
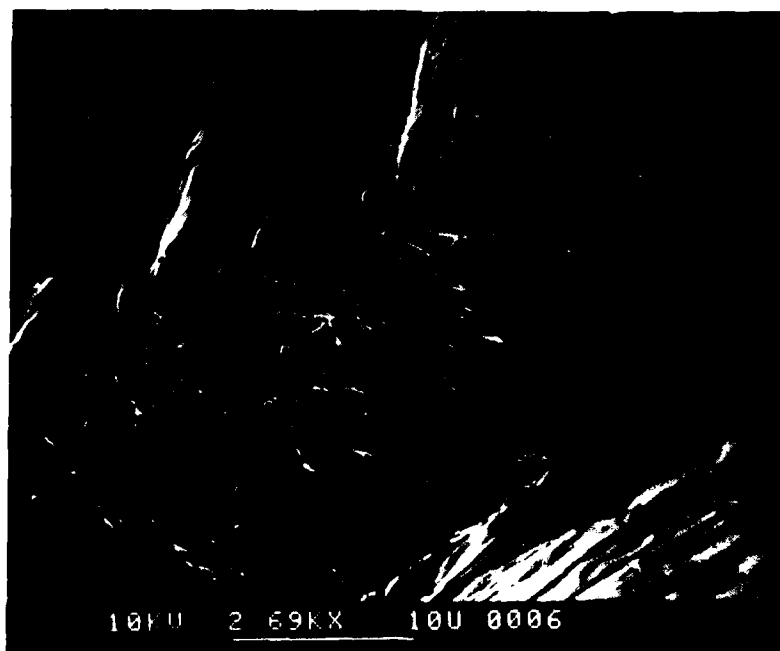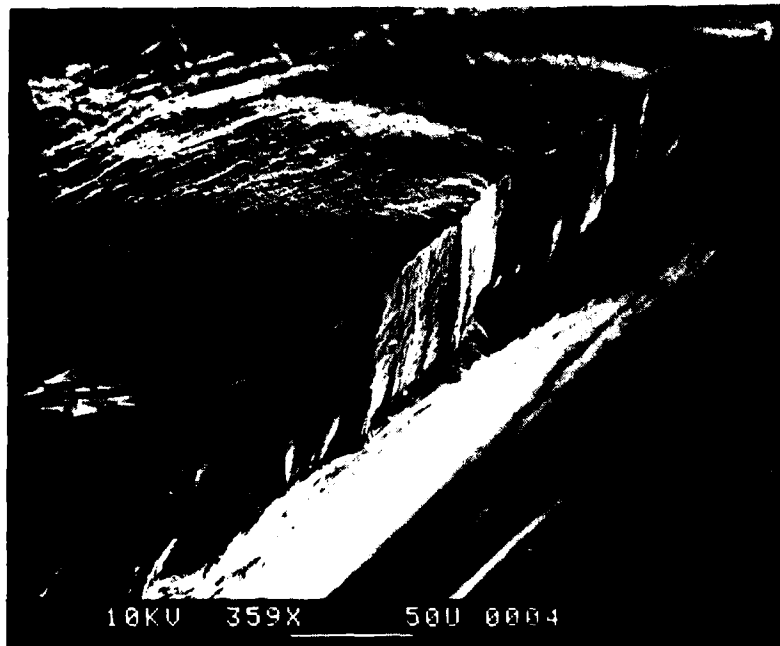
Figure 25.   Intergranular fracture surface of a hydrogen embrittled specimen fractured in liquid nitrogen.

Figure 26.   High magnification micrograph of a typical intergranular fracture surface showing shear steps and a great amount of relatively fine detail indicative of plastic processes.

10KV   86.4X   500U 0000

10KV   2.24KX   10U 0006
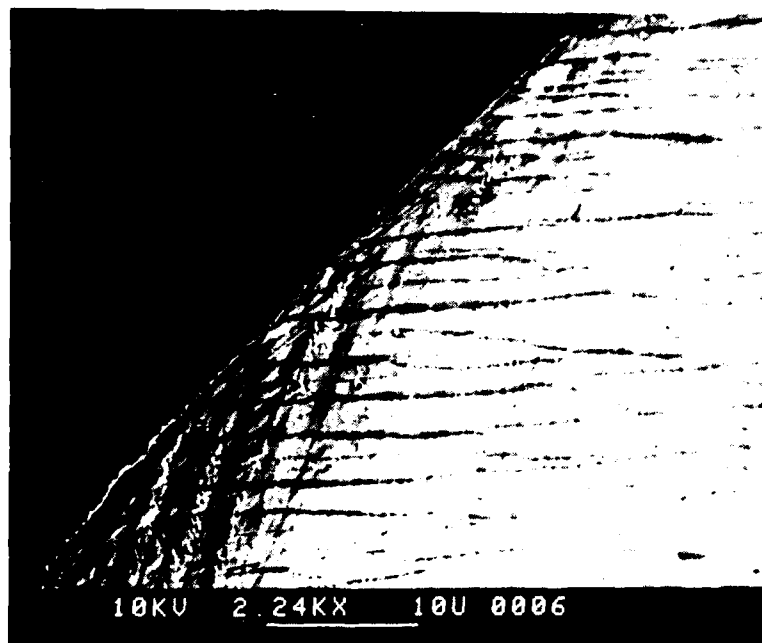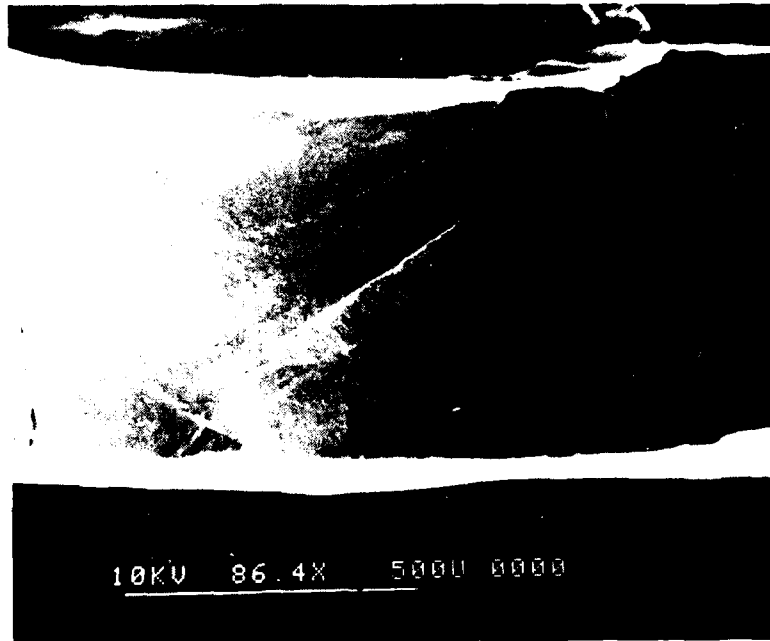
Figure 27.   Intergranular fracture surface with two sets of slip lines.
              Vertical lines are coarse, well defined and straight, diagonal
              traces are fine and wavy in nature.

Figure 28.   Micrograph of another intergranular fractu.e surface at about the
              same magnification of that shown in Figure 27. Multiple slip
              resulted in two sets of slip lines. Both sets are fine and wavy.
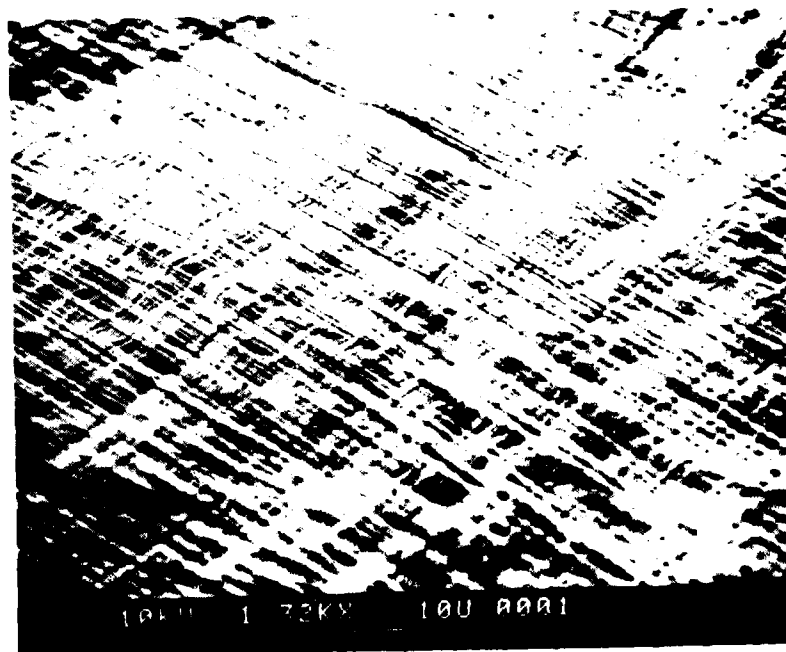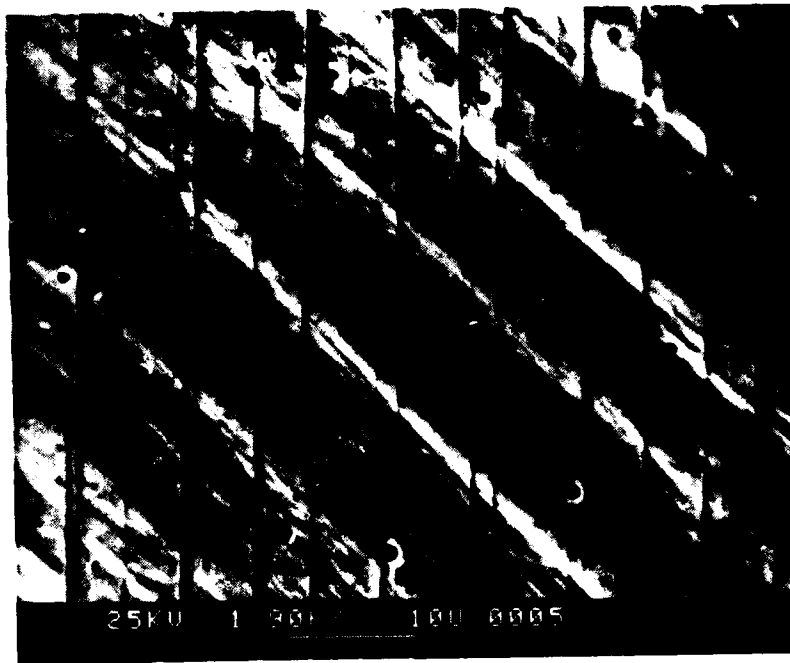
Figure 29.   Typical intergranular fracture surface of a NS2 tensile
             specimen. NS2 samples were shown to have a sulfur coverage of
             about 0.06 that extended on the order of 50 Å from the boundary.
             The fracture surface is relatively smooth and featureless in
             comparison to intergranular surfaces examined without large depths
             of sulfur coverage or sulfur free surfaces.

Figure 30.   Micrograph showing a band of holes on an intergranular fracture.
             Holes had matching holes on the mating surface indicating that
             they were spherical voids prior to fracture.

10KU   1 81KX   10U 0004

10KU   5 99KX   5U 0002

68
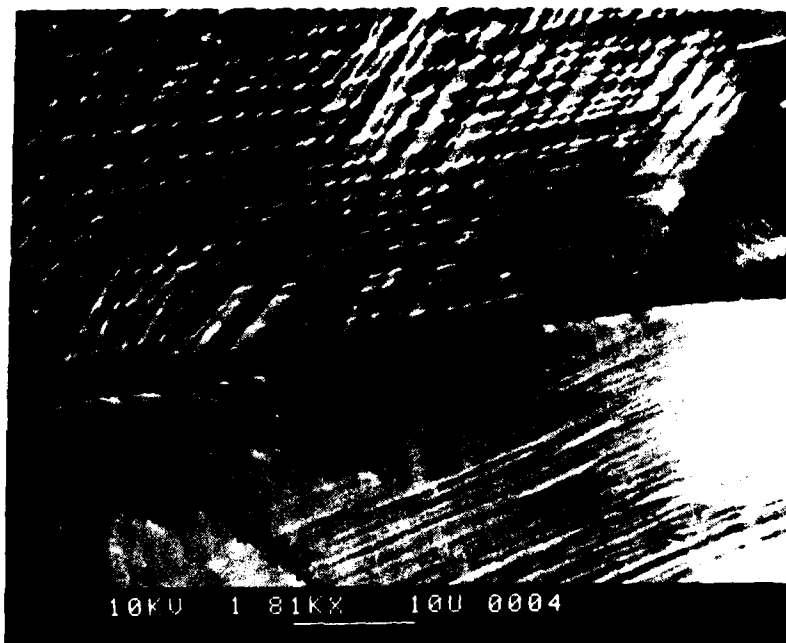
Figure 31.   TEM micrograph showing a hole in a sample that was annealed in a
              N-%5H$_2$ atmosphere for 1 hour at 1300°C.

Figure 32.   TEM micrograph of a hole in sample that was charged with hydrogen
              and aged at -65°C for 1.8 x 10^6 second. There is no evidence of
              void growth from hydrogen precipitation.

1 μM
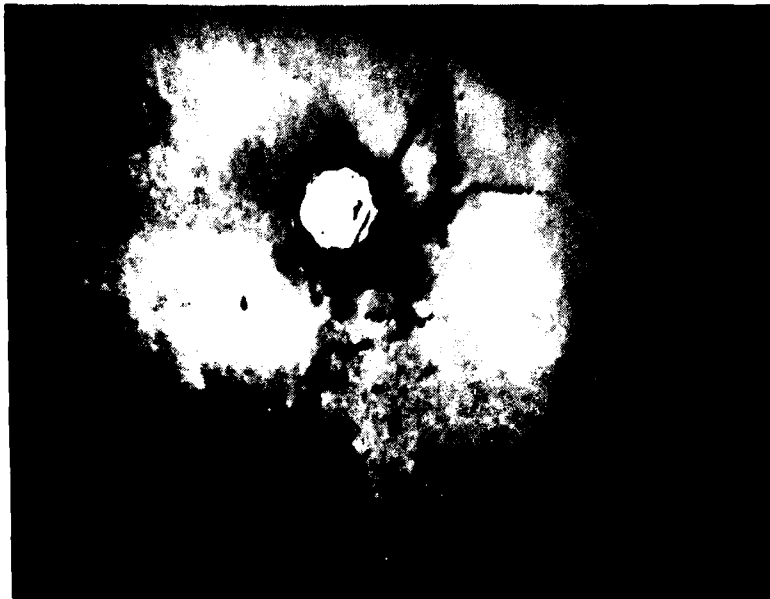
1 μM

CHAPTER 4

QUANTITATIVE ANALYSIS OF HYDROGEN SEGREGATION TO GRAIN BOUNDARIES

The thermodynamics and kinetics of hydrogen segregation to nickel grain boundaries are analyzed in this chapter. Values are obtained for the binding enthalpy of hydrogen to nickel grain boundaries and the thickness of the hydrogen enriched region at the grain boundaries.

4.1 Thermodynamics of Hydrogen Segregation

The dependence of fracture mode on bulk hydrogen concentration and aging temperature under quasi-equilibrium conditions (Figure 11) can be used to analyze the thermodynamics of hydrogen segregation to grain boundaries resulting in a value for the binding enthalpy of hydrogen to grain boundary traps. The analysis relies on the following assumptions; 1) aging temperature and bulk hydrogen concentration have no intrinsic effect on fracture mode, 2) that for a given percentage of intergranular fracture between 0% and 100% (100% > IG > 0%) the average concentration of hydrogen at grain boundaries is constant.

An expression for the equilibrium concentration of solute in a distorted region where trapping may occur, such as a grain boundary, has been derived by McLean[43]. The derivation of the model is based on the dependences of the free energy of the system on 1) the effect of solute trapping on configurational entropy and 2) the energy of a solute atom in a trap site with respect to an undistorted site in the lattice. The "McLean Equation" is derived by minimization of the free energy with respect to the concentration of solute atoms in trap sites and is as follows:

$$\frac{C_B}{1-C_B} = \frac{C_H}{1-C_H} \exp \frac{E-e}{kT} \tag{7}$$

where C_B is the fraction of trap sites which contain a solute atom, C_H is the fraction of solute atoms occupying lattice positions, E is the energy of a solute atom in the lattice, e is the energy of a solute atom in a trap, k is the Boltzmann constant and T is the equilibration temperature. The term E-e can be considered to be a binding enthalpy (ΔH_B) and will hereafter be referred to as such. If both C_B and C_H are much less than unity, only small errors will be introduced by simplifying equation to the following form;

$$C_B = C_H \exp \frac{-\Delta H_B}{kT} \tag{8}$$

The use of this equation relies on the bulk hydrogen concentration remaining essentially unchanged subsequent to quenching and on the assumption that the various values of bulk hydrogen concentration and aging temperature have no intrinsic effect on fracture mode. Conceivably there are two ways in which the initial concentration could be altered appreciably; by loss of hydrogen to traps (grain boundaries or traps in the bulk) and by outgassing (loss of hydrogen through the surface during aging procedures). It will be assumed that the bulk hydrogen concentration is unaffected by these losses. The validity of this assumption and the assumption that the various levels of solute hydrogen in the bulk have no intrinsic effect on intergranular fracture are more completely discussed in Appendix C.

Equation 8 can be applied to analysis of the data in Figure 11 by making the aforementioned assumption that for a given percentage of intergranular fracture the concentration of hydrogen at the grain boundaries is constant;

$$C_B = \text{Constant} = C_H \exp \frac{-\Delta H_B}{KT} \ . \tag{9}$$

The logarithm of the bulk hydrogen concentration is plotted for three levels of IG fracture at the respective aging temperatures in Figure 33. Least squares analysis of the data yielded values for the enthalpy of segregation equal to 0.12 eV (12 kJ/mole) with no significant variation in the values obtained at the different levels of IG fracture.

4.2 Kinetics of Hydrogen Segregation

It is intuitively obvious that as the aging temperature is decreased, longer aging times will be required to segregate a given quantity of hydrogen due to the decrease in diffusivity. The critical aging times for the three aging temperatures, plotted in Figure 10, supports this idea. Not so obvious is the effect of the binding enthalpy on the aging period required to attain a quasi-equilibrium condition. In this section the kinetics of equilibrium segregation of solute elements will be analyzed using diffusion theory and equation 8 to investigate the effect of diffusivity and binding enthalpy on hydrogen segregation.

Assuming that the depth of grain boundary enrichment is much smaller than the grain diameter and that the enriched region can be treated as a distinct phase, the problem can be dealt with as one of linear flow in a semi-infinite mass. The following equation, derived by McLean[43], treats the problem of solute segregtion as such;

$$\frac{C_{Bt} - C_o}{C_B - C_o} = 1 - \exp \left[\frac{4Dt}{\alpha^2 d^2} \right] \text{erfc} \left[\frac{2(Dt)^{1/2}}{\alpha \ d} \right] \tag{10}$$
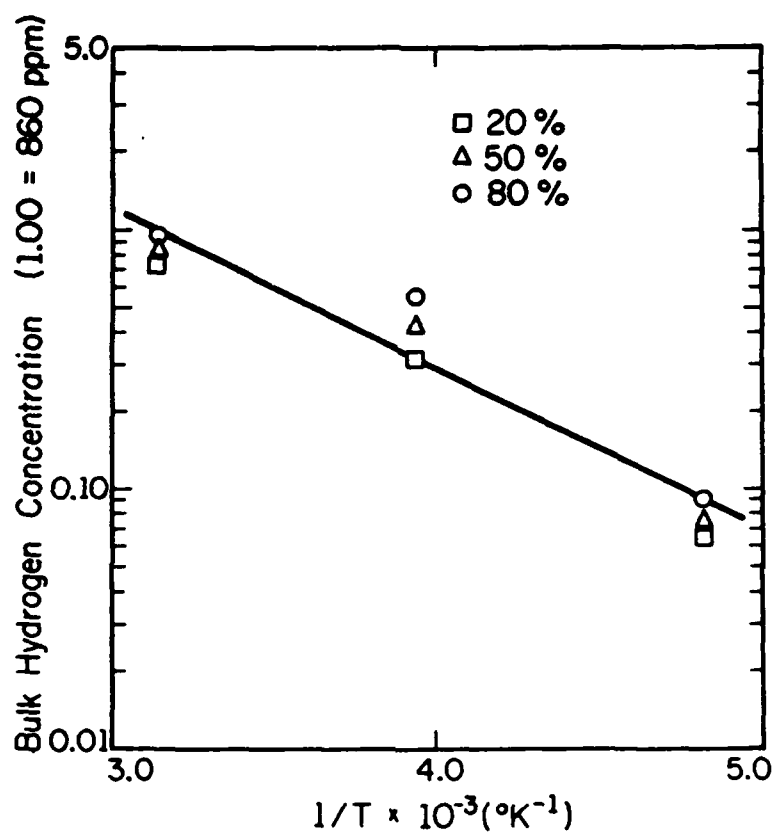
Figure 33. Bulk hydrogen concentration is plotted vs. reciprocal aging
temperature for three levels of intergranular fracture percent.
Least squares analysis of the data yield a value of 0.12 eV for
the hydrogen-grain boundary binding enthalpy.

where $\qquad$ C_{Bt} is the grain boundary concentration after time t

at the aging temperature

C_B is the quasi equilibrium grain boundary concentration

C_0 is the initial grain boundary concentration

C_H is the bulk hydrogen concentration

α is equal to $\exp \dfrac{-\Delta H_B}{kT}$

T is the aging temperature

D is the diffusivity at the aging temperature

d is the grain boundary thickness

A graphical representation of the idealized equilibrium solute enrichment profile at a grain boundary is givne in Figure 34.

The solution to equation 10 can be plotted as a function of $2\sqrt{Dt}/d\alpha$ as shown in Figure 35. To enhance the simplicity of the analysis we will assume that $C_0 << C_B$ such that the left hand side of equation 10 reduces to C_{Bt}/C_B at times approaching t_c. Figure 35 indicates that the grain boundary concentration builds up rather rapidly to a value of about 0.6 of the equilibrium value but the increase in concentration thereafter is relatively slow. Because of this factor a true equilibrium condition is impossible to attain in practice because of the eventual loss of hydrogen at the higher aging temperatures and the extremely long aging times required at low temperatures.

Equation 10 can be used to analyze the effect of aging time on grain boundary fracture in two ways; 1) to estimate the thickness of the hydrogen enriched region at the grain boundary and 2) to compare the known value for the activation energy for diffusion of hydrogen in nickel with a value calculated using the critical aging times.
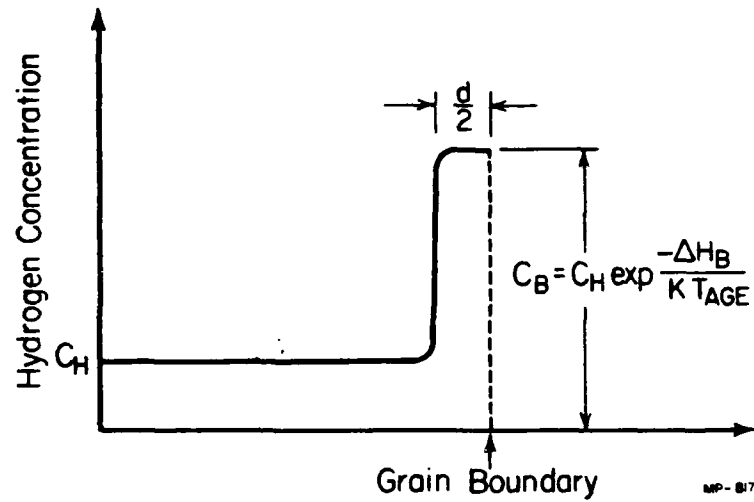
Figure 34.   Idealized profile of equilibrium hydrogen segregation at a grain boundary.

4.2.1 Hydrogen Enriched Region

To calculate the average breadth of the hydrogen distribution, d, at a grain boundary under quasi-equilibrium conditions it will be necessary to assume that a critical aging time corresponds to a value on the abscissa of the plot shown in Figure 34 (in essence to a value of grain boundary hydrogen enrichment, C_B/C_H). To do this it is useful to compare the shape of the curve in Figure 35 with the curves in Figures 8 and 9 showing the dependence of aging period on percent IG fracture. All curves show a region of rapid rise with a subsequent leveling off or slow rise of the plotted variable. Because of this it may be reasonable to assume that the quasi-equilibrium times correspond to a value of $2\sqrt{Dt}/\alpha d$ taken from Figure 35 of about 1.0 (C_{Bt}/C_B = 0.6), we can then write the following expression:

$$\frac{2\sqrt{Dt_c}}{\alpha d} = 1.0 \tag{11}$$

By substituting for D and α and rearranging we obtain the following expression for the effective thickness of the grain boundary with respect to hydrogen enrichment;

$$d = 2\ t_c^{1/2}\ D_0^{1/2}\ \exp \frac{-1}{kT_{age}}\ (\frac{Q_D}{2} - \Delta H_B) \tag{12}$$

The results of applying equation 12 to the data are given in Table 4 for the three aging temperatures. The values of d, in principle, should be about the same if physical parameters of the grain boundaries determine the breadth of segregation, however a variation of an order of magnitude is indicated. The value of d calculated from the critical aging time at the 45°C
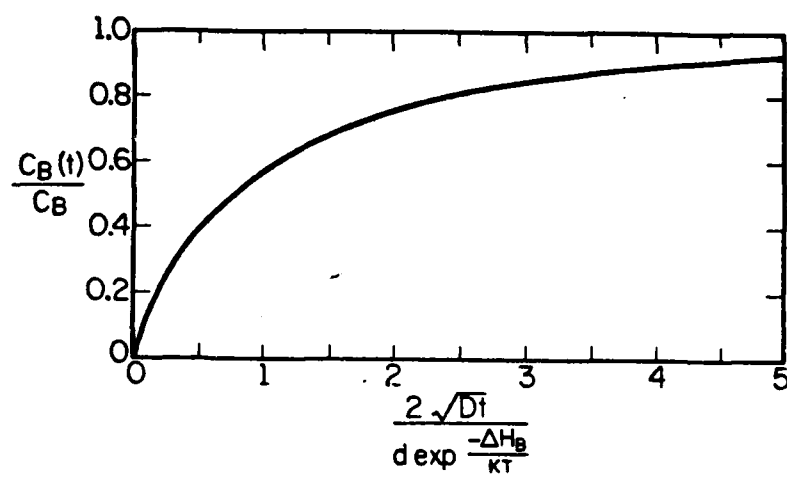
Figure 35. Normalized solute enrichment at grain boundaries vs. an aging parameter.

Table 4

Calculated Depths of Hydrogen Concentration Enrichment

$T_A(°C)$	t_c (sec)	d Å
45	200	1130
-20	10^4	350
-65	6×10^5	180

aging temperature is most likely much too large. This is due, in part, to the difficulties in estimating the point on the IG fracture vs. aging time plot for the 45°C aging temperature that has the value of C_{Bt}/C_B taken to be about 1.0 in the analysis. In any case the calculated value of d may be taken to be of the order of 350 Å with possibly some variation with aging temperature.

4.2.2 Analysis of Critical Aging Times

The critical aging time for a particular aging temperature represents the period of time required to maximize hydrogen segregation at grain boundaries and can be expressed by the following equation.

$$t_c = \frac{C \alpha^2 d^2}{D}$$

$$= [Cd^2] \exp \frac{-2 \Delta H_B + Q_D}{kT_a} \tag{13}$$

where C is a constant that depends on the value taken for C_{Bt}/C_B which at true equilibrium conditions will equal unity. By taking the logarithm of both sides of equation 13 we have

$$\ln t_c = \frac{-2\Delta H_B + Q_D}{k} \cdot \frac{1}{T_A} + \ln C + 2 \ln d \tag{14}$$

If we assume that d has a single value, independent of aging temperature, the logarithm of the critical aging time should vary linearly with the reciprocal of the aging temperature (1/T) and be proportional to $-2\Delta H_B + Q_D$, which equals 0.64 eV if ΔH_B equals 0.12 eV and Q_D is taken to be 0.4 eV. From Figure 10 the

experimental value of $-2\Delta H_B + Q_B$ equals 0.37 eV or roughly half the theoretical value. This variance is most likely due to 1) the over and/or underestimation of the critical aging times, and/or 2) the assumption that d is independent of temperature which may be an over simplification of the problem.

CHAPTER 5

DISCUSSION

The results of this study reveal much about the thermodynamics and nature of hydrogen segregation in the nickel hydrogen system in addition to adding considerably to the understanding of hydrogen embrittlement of nickel. The following sections will review, contrast and compare previous publications with the findings of this study. Section 5.3 of the discussion will deal with the proposal of an embrittlement mechanism drawing heavily from information provided by this work. This will be followed by discussion of hydrogen-sulfur cosegregation and conclusions.

5.1 Hydrogen Segregation

The depth of equilibrium segregation of impurity elements such as sulfur and phosphorous at nickel grain boundaries has been shown by AES analysis to extend for a distance on the order of a monolayer. This is in keeping with the traditional thought that equilibrium segregation occurs only in regions of lattice distortion since the distortion or disorder at grain boundaries extends only for about one monolayer[44]. The analysis of the kinetics of hydrogen segregation in this work suggests that a relatively thick layer of about 350 Å of hydrogen enrichment occurs about grain boundaries at equilibrium. Although this result is not consistent with direct observation of segregation of other elements, a study by Fukushima and Birnbaum[7] of the

segregation of hydrogen (deuterium) to surfaces and grain boundaries in charged nickel using SIMS (Secondary Ion Mass Spectroscopy) also suggests that hydrogen segregation can occur over appreciable distances. Fukushima suggests that this behavior is due to a long range attractive interaction between hydrogen atoms transmitted by the nickel lattice which is demonstrated by the miscibility gap in the Ni-H phase diagram.

The value of the binding enthalpy of hydrogen to grain boundaries determined in this work compares quite favorably with other studies of the binding to point defects and dislocations in nickel and other fcc metals. The following table summarizes some experimental and theoretical results along with the present result.

Table 5

Values of Hydrogen-Defect Binding Enthalpies in Nickel

Defect	ΔH_B (eV)	Ref
Grain boundary	-0.12	this work
Dislocation	-0.08	Boniszewski (1)
Vacancies	-0.05	Baskes (45)
Ti, Fe impurities	-0.1	Thomas (46)
Incoherent oxide	-0.3	Robertson (47)

As stated previously, the result of the negative grain boundary-hydrogen binding enthalpy is to increase the concentration of hydrogen at boundary trap sites with respect to the bulk hydrogen concentration. To illustrate the equilibrium enrichment of hydrogen concentration at grain boundaries,

C_B/C_H is plotted as a function of aging temperature in Figure 36. Large increases in grain boundary concentration will occur at low temperatures, for example an enrichment of 1100 occurs at -65°C, with decreasing amounts at higher temperatures. From an experimental standpoint there will be a limit on equilibrium hydrogen enrichment because of the requirement of exceedingly long aging periods. A limit may also be imposed due to hydride formation.

Within the bounds of the experimental parameters of this work (-65 < T_{age} < 45°, -196 < T_{test} < -65°C) it is possible to determine the relationships between grain boundary hydrogen concentration and percent intergranular fracture. This is done by considering the equilibrium enrichment that occurs at a given aging temperature and the experimental relationship between intergranular fracture and bulk hydrogen concentration. A plot of percent intergranular fracture versus grain boundary hydrogen concentration (Figure 37) was determined using the quasi-equilibrium fracture data generated utilizing the -20°C aging temperature (Figure 11). The curve is sigmoidal in nature, rising at a hydrogen concentration of 10% and then saturating (100% intergranular fracture) at about 20% hydrogen concentration. It should be noted that it is impossible to attain these levels of bulk hydrogen concentration by thermally charging in one atmosphere of hydrogen gas. Consequently segregation must occur if any intergranular fracture is to result.

The intergranular fracture mode requires that a critical hydrogen concentration be attained at a grain boundary along the fracture path, the value of which will depend on stress components applied to the boundary and the nature of the boundary itself (i.e. the nature of the boundary may affect the degree of segregation that occurs under a given aging condition and the
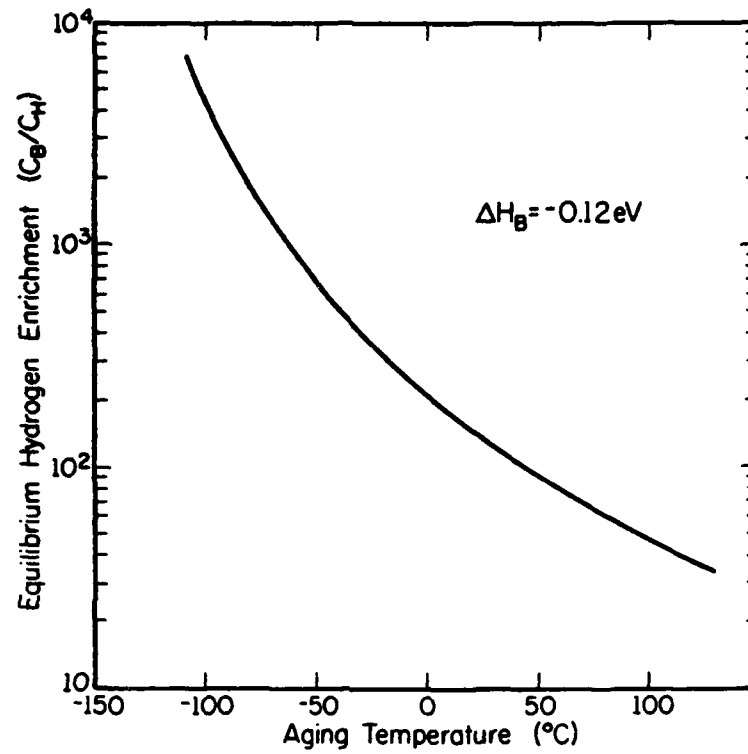
Figure 36.   Equilibrium grain boundary hydrogen enrichment vs. aging time. Actual enrichment of hydrogen may be limited by diffusivity or hydride formation.
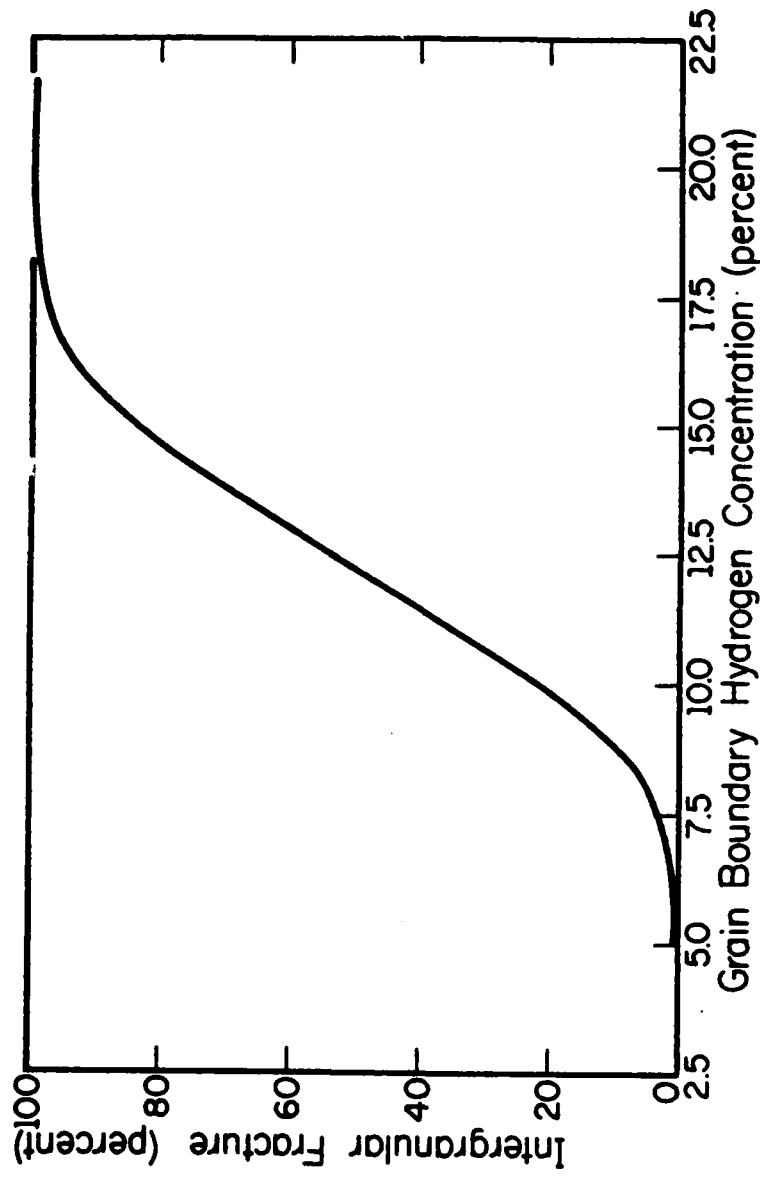
Figure 37.   Percent intergranular fracture vs. grain boundary hydrogen concentration.

fracture strength of the boundary). Upon testing after an aging treatment, those boundaries which have achieved the critical concentration for their particular local stress condition will fracture and thus contribute to the embrittlement. As an aging period ($t_{age} < t_c$) or the bulk hydrogen concentration is increased, a greater number of boundaries will attain their particular critical concentration, leading to a more complete intergranular fracture mode and to maximum embrittlement. The behavior of polycrystalline specimens such as are used in the present study reflect an averaging over the types of grain boundaries and their orientations relative to the applied stress along the fracture path, thus resulting in a range of grain boundary hydrogen concentration for values of intergranular fracture between 0 and 100%.

5.2 Hydrogen Embrittlement

The results of this study clear up much of the confusion regarding the test temperature and strain rate dependence on the embrittlement of nickel. Diffusive segregation to grain boundaries and subsequent enrichment has been shown to play a primary role in conditions which lead to embrittlement. As a result parameters which affect diffusive segregation, aging period and temperature, are fundamental. This statement can be best expressed by the following qualitative expression

$$\text{Embrittlement} = f(C_H, t_{age}, T_{age})$$

Previous works on the hydrogen embrittlement of charged nickel have investigated in detail the effect of strain rate and test temperature on

embrittlement. For a given strain rate a ductility minimum has been reported to occur at a test temperature of about -50°C with a return to ductile behavior at either higher or lower test temperatures. Embrittlement has been shown to be more severe at slow strain rates when testing is performed at temperatures that allow some degree of hydrogen mobility.

These observations can be explained rather simply if one considers the effects of strain rate and test temperature on the diffusive segregation of hydrogen to grain boundaries. Firstly, as the strain rate is decreased the aging period that occurs during testing increases and results in an increasing amount of intergranular fracture provided $t_{age} < t_c$. This is illustrated quite vividly by the data presented in Figure 13 which shows the embrittling effect of reducing the strain rate three orders of magnitude at -65°C due to aging that occurs during testing. The effect of strain rate on aging will diminish at higher and lower temperatures. At higher temperatures the critical aging time will be exceeded at even the fast strain rates. Consequently, going to a slower strain rate will not increase hydrogen enrichment at grain boundaries. For example t_c equals about 240 seconds at 45°C. At a strain rate of 10^{-2}, a typical test will take about this long if set up time is included. At lower test temperatures the effect of strain rate on diffusive segregation will be small (provided the specimen is quenched to the test temperature) because of the decreasing diffusivity of hydrogen resulting in small amounts of enrichment for even long periods of aging time during testing.

A semi-quantitative figure, after Windle and Smith[5], showing the effect of test temperatures on embrittlement for a constant strain rate is shown in

Figure 38. As the test temperature of a tensile test is lowered, the degree of segregation is increased if the duration of the test is greater than or equal to t_c. As a result, at higher test temperatures where t_c is relatively short, equilibrium behavior with respect to the embrittling effect of diffusive segregation will be observed. However at lower temperatures, the samples tested in Windle and Smith's work were not aged sufficiently long to attain a quasi-equilibrium condition, as a result a return to ductile behavior is observed. Equilibrium behavior is depicted in a qualitative sense by the dashed line in Figure 38.

To sum up this section, it is clearly evident that the parameters strain rate and test temperature affect the fracture by means of their effect on hydrogen segregation to grain boundaries, strain rate corresponds to aging time and test temperature to aging temperature. As the strain rate is decreased the aging period is increased; as the test temperature is decreased aging temperature is decreased, resulting in a greater embrittlement tendency under some conditions.

5.3 Embrittlement Mechanism

When evaluating the embrittling effect of hydrogen and attempting to determine the embrittlement mechanism three major physical parameters must be considered; 1) the source of hydrogen, 2) the transport of hydrogen and 3) trapping of hydrogen. The following paragraphs will evaluate these factors for the embrittlement of hydrogen charged nickel.

a) Source of hydrogen

The source of embrittling hydrogen during deformation or sustained load failure may be internal or external to the material. Examples of external sources are gaseous hydrogen, corrosion reactions and cathodic charging.
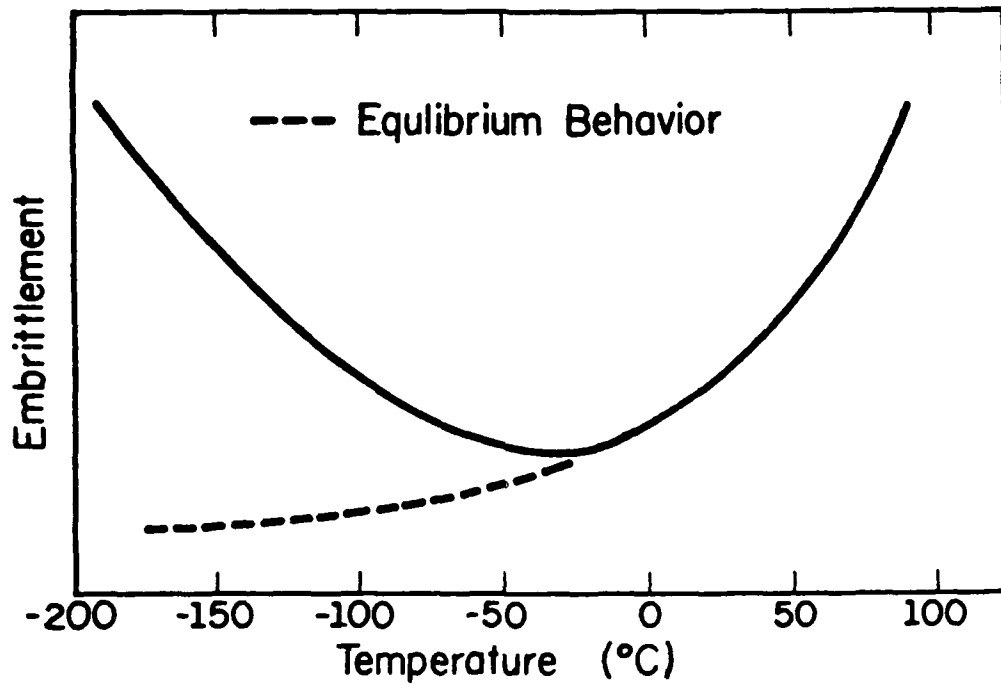
Figure 38. Embrittlement of hydrogen charged nickel vs. test temperature (after Windle and Smith[5]). Dashed line shows embrittlement behavior if a quasi-equilibrium condition with respect to grain boundary hydrogen segregation is attained prior to fracture.

"Internal source" refers primarily to hydrogen in solution as a result of thermal or cathodic charging prior to embrittlement. In this study samples were thermally charged, (the source was internal) which resulted in a highly supersaturated solution of hydrogen in nickel. If thermodynamic and kinetic conditions are favorable, supersaturation may result in precipitation of a hydride phase or hydrogen bubbles; either of which are potential embrittlement mechanisms. In this work no direct physical evidence of a hydride phase such as that reported by Szummer et al.[17] or bubble growth due to the precipitation of molecular hydrogen was obtained.

b) Transport

Transport of hydrogen in nickel can occur by dislocation transport or lattice diffusion. In this work the dislocation transport of hydrogen during testing has been shown not to be actively involved in the embrittlement mechanism for test temperatures at or below -65°C i.e. embrittlement is not dependent on hydrogen mobility during the fracture process.

c) Trapping

Trapping of hydrogen at grain boundaries has been shown to be of primary importance in the embrittlement of nickel. Despite the weak hydrogen-grain boundary binding enthalpy, considerable enhancement of hydrogen occurs even at temperatures as high as 45°C. This and other work[7] suggests that the hydrogen rich region extends appreciable distances (350 Å) from grain boundaries.

It can be noted at this point that since hydrogen trapping at grain boundaries has been shown to be necessary and sufficient with respect to embrittlement, competitive trapping may serve to alleviate embrittlement of charged material to some extent. In a work by Thompson and Wilcox[47] dispersed thoria has been shown to reduce embrittlement susceptibility of

END
FILMED

DTIC
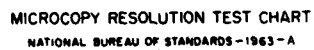
MICROCOPY RESOLUTION TEST CHART

NATIONAL BUREAU OF STANDARDS-1963-A

charged nickel; most likely due to the innocuous trapping of hydrogen at thoria particles, thus reducing bulk hydrogen concentration.

At this time the detailed mechanism of the intergranular fracture process can only be guessed. However considering the facts presented above, some mechanisms can be discarded; for example a high pressure bubble mechanism or mechanisms that require some degree of hydrogen mobility.

Because of the relatively high calculated hydrogen concentration in the volume in which the fracture occurs and the fact that hydrogen need not be mobile, the possibility remains that embrittlement is due to a hydride phase. The only documented observations of nickel hydride have characterized the phase as hard and brittle much like other metallic hydrides such as those formed by niobium and titanium. There are several points in variance with a "brittle" hydride mechanism based on observations made of fracture surfaces and the dynamics of the fracture process. Firstly, the intergranular fracture surface of embrittled nickel (Figures 27, 28) appear to have much detail that is indicative of plastic processes. This may be compared to the brittle, relatively featureless appearance, of a cleaved titanium or niobium hydride, or the intergranular fracture of a sulfur laden nickel grain boundary such as shown in Figure 29. In addition, large amounts of grain boundary sliding occur during the intergranular fracture process. Figure 39 shows a grain boundary separation that occurred remote from the main fracture in a Ni-xx specimen tested in liquid nitrogen. A large uniform displacement of the fracture surfaces indicates considerable sliding had occurred in adjacent boundaries. Vivid evidence of grain boundary sliding in embrittled nickel has also been provided by Heubam[6] who studied the dynamics of the fracture process in situ in a SEM. Video tapes made of intergranular cracks advancing

Figure 39.   SEM microcrack of a hydrogen related crack which opened in an area
              remote from the main crack. The large and uniform crack opening
              displacement and intense shear bands indicate a great deal of
              grain boundary sliding occurred subsequent to fracture.

show that large amounts of grain boundary sliding in boundaries preceded the crack tip. These observations indicate that the intergranular fracture associated with hydrogen embrittlement of nickel is not a result of the fracture of a brittle nickel hydride.

Since the intergranular fracture appears to be due to local plastic processes at boundaries it is proposed that intergranular fracture is caused by a region extending about 350 Å from grain boundaries that is softened by the presence of about 15% hydrogen concentration. This region conceivably has a low yield strength and work hardening rate with respect to nickel with only moderate amounts of hydrogen in solution (C_H < 0.1%) such as that used in this study. During axial deformation grain boundary fracture occurs as a result of the deformation and crack growth in the softened region.

5.4 Effect of Sulfur-Hydrogen Cosegregation

The results of nickel tested with various amounts of sulfur present at grain boundaries indicate that the effect of about one tenth of a monolayer of sulfur is not a cause in and of itself for embrittlement. In combination with trace amounts of hydrogen this amount of sulfur segregation will however cause considerable grain boundary fracture. This is evidenced by the intergranular fracture obtained after specimens were heated to 850°C in a wet argon atmosphere (which introduced hydrogen by reaction of the nickel with H_2O) and then quenched into water. Completely ductile fracture resulted when a specimen was held in a vacuum at 850°C, thereby outgassing any trace amounts of hydrogen, and was then quenched into oil. Because the partial pressure of hydrogen in the wet argon atmosphere would be expected to be very low resulting in a very low bulk hydrogen concentration of a quenched sample, it is suggested that significant amounts of hydrogen were bound to sulfur at the quench temperature and that

this hydrogen acted additively or in a synergistic fashion with sulfur promoting grain boundary fracture. The segregation of hydrogen to sulfur in nickel at temperatures as high as 572°C has been reported by Fukushima[7]. The above proposal agrees with this finding but the results of this work offer no direct evidence by itself.

5.5 Conclusions

Experiments were carried out to study the effects of grain boundary segregation of hydrogen on the fracture mode of nickel and nickel with various amounts of grain boundary sulfur segregation. The effect of strain rate and presumably dislocation transport on embrittlement was also studied. The major conclusions of this work are summarized below.

a) It has been shown that the accumulation of sufficient quantities of hydrogen at grain boundaries by diffusive segregation will result in a change in the fracture mode of nickel from ductile shear rupture to the intergranular mode. Parameters affecting diffusion and trapping of hydrogen in nickel play a major role in conditions which lead to embrittlement (eg. aging temperature and aging time).

b) The hydrogen-grain boundary binding enthalpy has been calculated to be 0.12 eV (12 kJ/mole) based on the fracture mode dependence on bulk hydrogen concentration and aging temperature. This binding enthalpy results in appreciable amounts of hydrogen concentration enhancement at temperatures as high as 45°C.

c) An analysis of the kinetics of hydrogen segregation suggests that hydrogen enhancement extends to distances from the grain boundary on the order of 350 Å.

f) It is suggested that the mechanism of hydrogen embrittlement of nickel is the deformation and fracture of a relatively soft region at grain boundaries. The proposed soft region is associated with a local hydrogen concentration of about 15% extending on the order of 350 Å from grain boundaries.

g) Grain boundary sulfur segregation on the order of 0.1 monolayer has been shown to severely increase the embrittlement susceptibility of hydrogen charged nickel.

Appendix A

This appendix consists of tables which contain specimen preparation and test data. All specimens tested are included. Table A1 lists Ni-xx specimens. Table A2 lists ND-xx specimens. Tables A3, A4 and A5 list NS1-xx, NS2-xx and NS3-xx specimens respectively.

Table A1

Ni-xx	C_H 1.0= 860 ppm	T_{age} °C	t_{age} sec	%IG	%e	σ_f MPa
7	.89	-20	8.6×10^4	100	18	327
8	.77			95	22	351
9	.69			90	25	406
10	.51			60	26	376
11	.36			40	20	340
12	.28			10	24	364
13	.20			0	38	436
15	.51		10^4	75	25	364
16			10^4	60	27	388
17			10^3	20	34	467
18			10^3	30	23	358
19			4×10^3	50	22	376
20			4×10^3	45	31	442
21			10	10	25	351
23			2.4×10^5	50	17	291
24			4.6×10^4	80	31	442
26	.32		4.2×10^4	15	33	442
27			4.2×10^4	15	30	442
28			2.4×10^5	15	26	370
29			2.4×10^5	25	24	364
30			1.4×10^4	10	32	448
33			10^2	5	29	412
34			10^2	0	30	430
36			10^3	10	30	412
37			10^4	25	19	---
38			10^4	40	32	---
39	.77		10^4	85	21	333
40	1		10^4	100	13	236
41	.77	-20	10^2	85	19	309
42	.77		10^2	100	25	406
43	.77		10^3	95	17	279
44	.77		10^3	100	--	---
45	.05	-65	6×10^5	5	33	467
46	.11			95	21	352

N1-xx	C_H 1.0= 860 ppm	T_{age} °C	t_{age} sec	%IG	%e	σ_f MPa
47	.19	-65	6×10^5	100	--	---
49	.28			95	11	194
50	.51			100	--	---
51	.63	45		100	--	---
53	1.0	45	240	95	28	364
54	1.0			100	23	382
55	.89			75	28	430
56	.89			55	35	467
57	.77			50	--	352
58	.77			25	21	315
59	.77			35	33	455
60	.77			40	25	354
61	.89		10^2	30	31	382
62	.89		10^2	70	29	424
63	.89		10^3	85	20	351
64	.77	-20	10	60	--	---
65	.77	-20	10	85	--	---
66	.89	45	10^3	70	--	---
67	.89		2.6×10^5	20	30	430
68	.89		2.6×10^5	10	33	479
70	.63	45	240	0	--	---
71	.11	-65	10	0	46	509
72	.11		10^2	0	34	442
73	.11		10^3	0	--	442
74	.11		10^4	0	44	497
75	.11		10^4	15	32	388
76	.89	45	4×10^3	85	22	345
77	.11	-65	4.3×10^4	70	33	382
78	.11		8.6×10^4	65	36	467
79	.11		2.6×10^5	70	--	236
80	.05		1.8×10^6	15	24	345
81	.11		1.8×10^6	100	14	267
82	.51	-20	10^2	25	26	364
83	0	-20	10^4	0	36	485

Table A2

ND-xx	C_H 1.0= 850 ppm	t_{age} (sec)	T_{age} (°C)	$\dot{\epsilon}/3.0$	%IG	%e	σ_f MPa
1	.11	---	---	10^{-5}	0	55	293
2	.11	6×10^5	-65	10^{-2}	95	34	293
3	.11	6×10^5	-65	10^{-5}	70	37	281
4	.28	---	---	10^{-5}	5	44	288
5	.51	---	---	10^{-5}	95	39	305
6	.51	7×10^3	-65	10^{-2}	100	---	---
7	.36	---	---	10^{-2}	0	48	332
8	.51	---	---	10^{-2}	0	45	351
9	.36	---	---	10^{-5}	5	30	260
10	.63	---	---	10^{-2}	10	41	306
11	.89	---	---	10^{-2}	50	38	306
12	.36	---	---	10^{-5}	50	28	243
13	.63	---	---	10^{-5}	100	31	256
14	.36	7×10^3	-65	10^{-2}	60	31	281
15	.63	7×10^3	-65	10^{-2}	95	28	243
16	.28	7×10^3	-65	10^{-2}	60	42	306

$T_{test} = -65°C$

Table A3

NS1-xx	C_H 1.00= 600 ppm	t_{age} (sec)	T_{age} (°C)	%IG	%e	σ_f MPa
1	1.0	1.3×10^4	-20	100	17	321
2	1.0		-20	100	15	309
3	.89		-20	90	22	375
4	.77		-20	85	15	291
5	.63		-20	100	26	412
6	.51		-20	85	24	37ᶠ
7	.36		-20	70	23	3´
8	.28		-20	95	27	4
9	.21		-20	95	34	467
10	.11		-20	75	25	394
11	0		-20		broke at grip	
12	.05		-20	25	32	436
13	0		-20	25	27	448
14	.05	3×10^2	45	40	--	---
15	.11		45	50	36	467
16	.21		45	65	33	436
17	0	1.3×10^4	-20	0	39	479
18	.36	3×10^2	45	35	34	455
19	.51		45	15	30	455
20	.28		45	10	36	485
21	.77		45	50	32	442
22	.63		45	25	33	467
23	1.0		45	95	32	461
24	.89		45	10	25	430

$\dot{\varepsilon} = 3.3 \times 10^{-4} \text{ sec}^{-1}$, $T_{test} = -198°C$

Table A4

NS2-xx	C_H 1.0= 600 ppm	t_{age} (sec)	T_{age} (°C)	%IG
1	Vac	1.3×10^4	-20	100
2	Ar			100
3	.05			100
4	.11			100
5	Vac			100

All specimen quenched in oil, T_{test} = -198°C, $\dot{\varepsilon}$ = 3.3 x 10^{-4} sec^{-1}

Table A5

NS3-xx	C_H 1.0= 600 ppm	t_{age} (sec)	T_{age} (°C)	%IG	%e	σ_f MPa
1	Ar	1.3×10^4	-20	0	32	476
2	1.0			100	16	306
3	.11			0	30	464
4	.20			5	31	462
5	.36			broke at grip		
6	.51			25	27	476
7	.63			80	22	408
8	.77			95	18	226
9	.89			80	20	330

T_{test} = -198°C, $\dot{\varepsilon}$ = 3.3x10^{-4} sec^{-1}

Appendix B

Grain Boundary Chemical Analysis

Scanning Auger electron spectroscopy (AES) was used to determine the amount of sulfur at grain boundaries of the three batches of samples doped with sulfur (NS1, NS2, NS3). Results, which are summarized in Table 2, show that the three batches of specimens are significantly different in terms of sulfur coverage and depth of segregation adjacent to the boundaries.

B.1 AES Equipment and Procedure

A PHI model 595 scanning AES system was used to analyze elements whose concentration exceeds 1 percent in about a 1 μm diameter area to a depth of a few atomic layers. Depth profiles were obtained by repeatedly sputtering the sample with an argon ion beam and then recording the Auger spectra. The measurements were performed under the following conditions.

Primary energy	3000 eV
Electron beam current	20 nA
Beam diameter	1 μm
System pressure	2 x 10^{-10} Torr
Ion beam voltage	1000 V
Ion beam diameter	0.5 mm

To determine the relative sensitivities of the nickel and sulfur peaks in the Auger spectra under these operating conditions, a NiS_2 standard was analyzed. The NiS_2 standard consisted of NiS_2 powder which was pressed on to an indium sheet. Several points on the standard were sputtered to remove an oxide layer and than analyzed. A typical Auger spectra is given in Figure B1. The Ni/S sensitivity factor ($S_{Ni/S}$) was calculated using the following equation.

$$S_{Ni/S} = \frac{P_S}{P_{Ni}} \cdot \frac{Ni}{S}$$

B1

where P_{Ni} and P_S are the 156 eV and 860 eV peak heights for nickel and sulfur respectively, and Ni/S is the nickel to sulfur ratio of the standard.

Auger specimens, NS1, NS2 and NS3, were prepared from NS1, NS2 and NS3 tensile specimens. Because sulfur, oxygen and carbon from the atmosphere will quickly adsorb on clean nickel surfaces and will then make obtaining the Auger spectra difficult, several steps were taken to facilitate in situ inter- granular fracture: samples were first prestrained in tension to about 30% in liquid nitrogen and then notched with a jeweler's saw. Samples were then cathodically charged with hydrogen for about 4×10^4 seconds in a solution of 5% H_2SO_4 and 95% H_2O with 0.25 gm/l $NaAsO_2$ added as a hydrogen recombination poison. The current density used during cathodic charging was 20 $\mu A/cm^2$. Samples were then mounted in a cold fracture stage in the AES and cooled to about -40°C for about 12 hours prior to fracture to segregate hydrogen to grain boundaries. This procedure resulted in large amounts of intergranular fracture subsequent to impact loading in situ at a base pressure of 2×10^{-10} Torr. Insignificant amounts of contamination occurred during the period of time required to analyze fracture surfaces.

B.2 Results

The depth profile results obtained from sample NS1 are shown in Figures B2, B3 and B4. The initial surface coverage was calculated to be 0.06 using equation B1. The depth of coverage was estimated to be on the order of one monolayer based on the comparison of the sputtering time required to reduce the sulfur signal to noise levels and the sputtering time required to remove adsorbed carbon and oxygen from a sample exposed to air prior to analysis.

Sulfur coverage was mapped for a matching pair of fracture surfaces on sample NS1. Within the resolution of the experiment it was determined that there was uniform and equal sulfur coverage on the fracture surfaces. This result suggests that the mean intergranular fracture path deviates little from the grain boundary.

Figures B5, B6 and B7 show results of the depth profiling of a NS2 specimen. The ratio of the nickel and sulfur peak heights is about the same as of the NS1 specimen indicating the sulfur coverage was about 0.06 of a monolayer. The depth of coverage was shown to be considerably greater than that observed in sample NS1. Based on the comparison of sputtering times necessary to irradicate the sulfur signals of specimens NS1 and NS2, it is estimated that the depth of segregation extends about 50 Å on both sides of grain boundaries in NS2 specimens. This extended region of S may result from the method of preparation of these specimens. Sulfur was diffused in from the vapor phase and rapid diffusion along grain boundaries followed by sulfur diffusion into the grain interiors would produce the observed extended region of sulfur segregation. In any case, the segregation is non-equilibrium since equilibrium segregtion extends on the order of only a few atomic distances[44].

Sample NS3 was fractured in situ and analyzed for sulfur at grain boundaries. The analysis of many points indicated that the boundaries were essentially free of sulfur. A typical AES spectrum is shown in Figure B8. Depth profiling was not performed on this sample because the fracture surfaces available for analysis after breaking the sample were not favorably oriented for sputtering.

Figure B1.   Auger spectra of NiS_2 compound. The ratio of the labeled nickel and sulfur peaks was used to determined the sensitivity factor.

Figure B2.   Auger spectra of sample NS1 before sputtering with an argon ion beam. Sample was fractured in situ in a vacuum of 3×10^{-10} Torr. Sulfur coverage is about 0.06.

AES   SURVEY   SF= 4.969, -36.192 DAT= 5.00   05/16/84 NIS2A   P-C

NiS₂ STANDARD SPECTRA

KINETIC ENERGY, EV

AES   SURVEY   SF= 12.480, .000 DAT= 5.00   04/04/84 NS15A   P-C

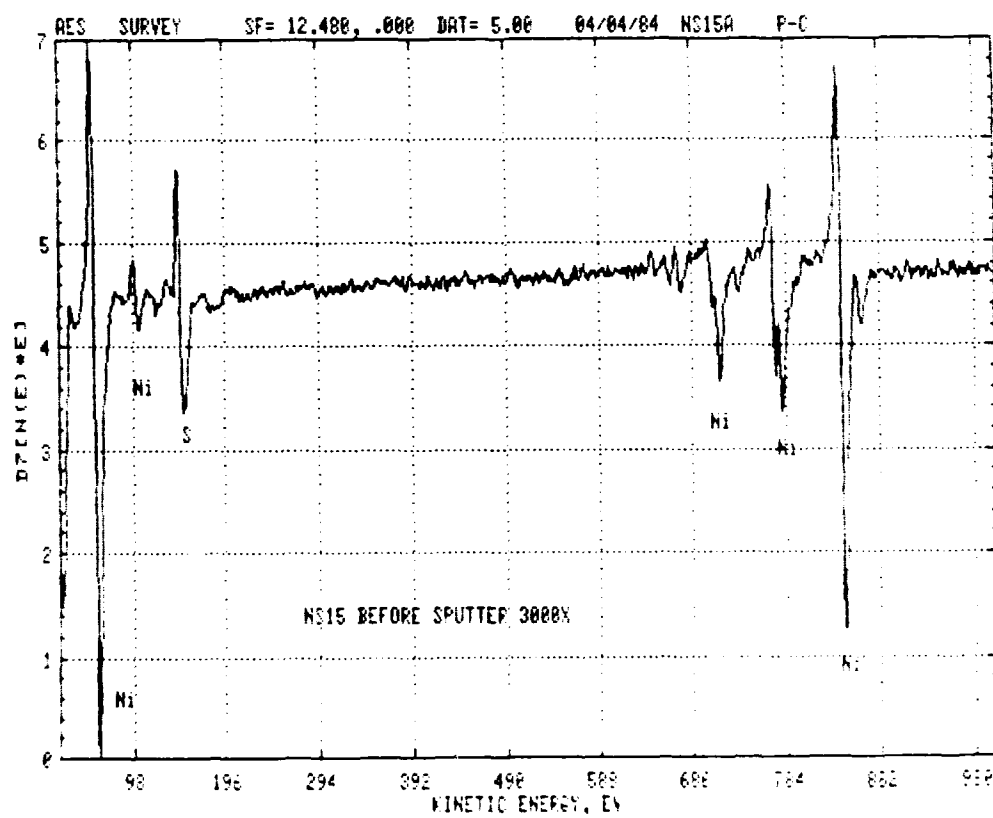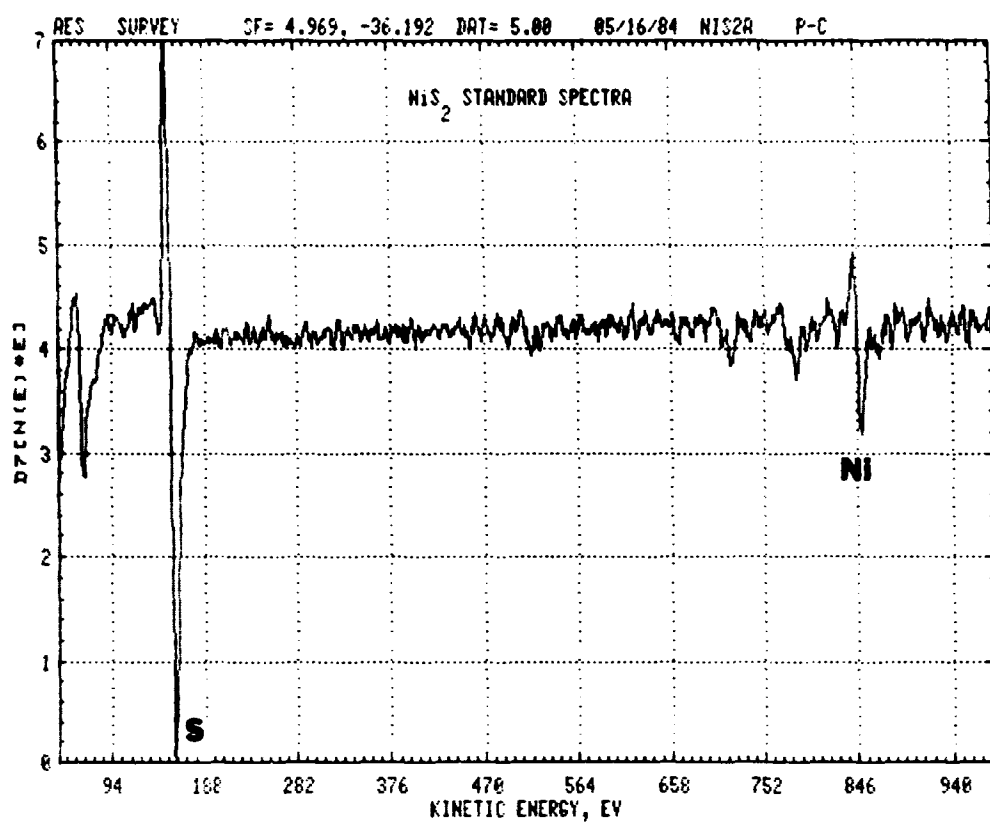NS15 BEFORE SPUTTER 3000X

KINETIC ENERGY, EV

Figure B3. Depth profile of sample NS1, which shows the Auger peak heights of
nickel and sulfur vs. sputtering time. The sputtering time needed
to irradicate the sulfur signal indicates that about one monolayer
of sulfur was present before sputtering.

Figure B4. Auger spectra of sample NS1 after depth profile. A small amount
of Ar, C and O contamination of the sample occurred during
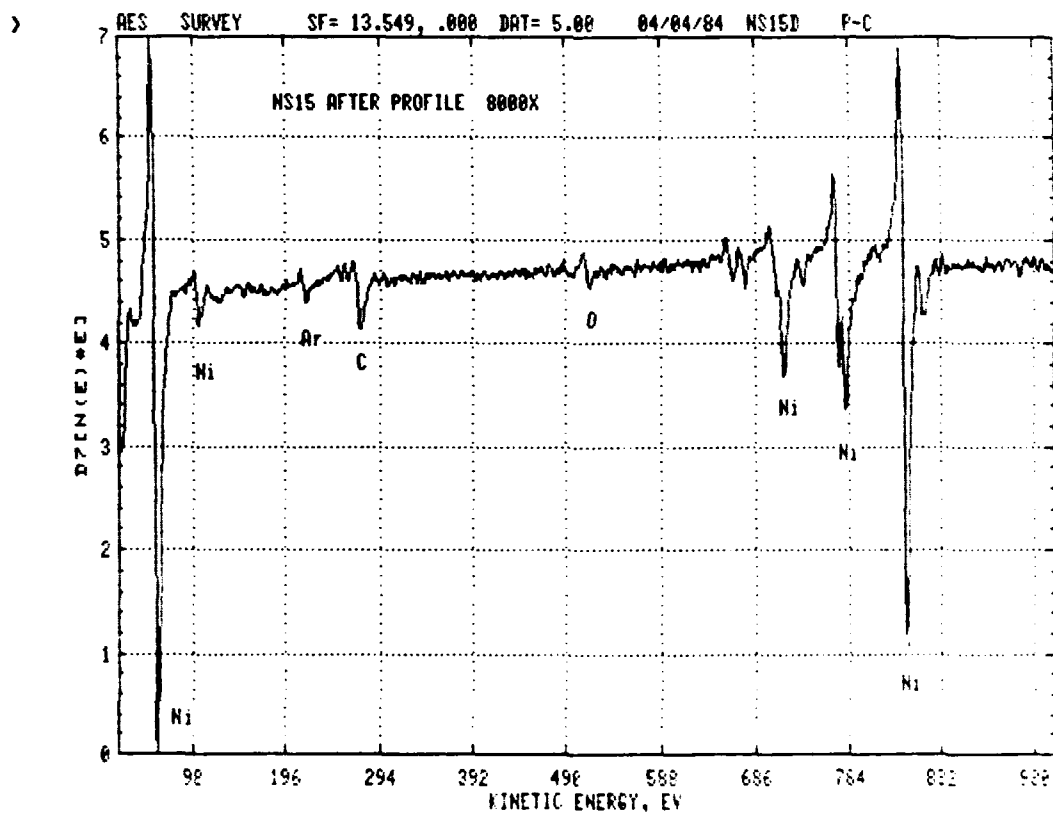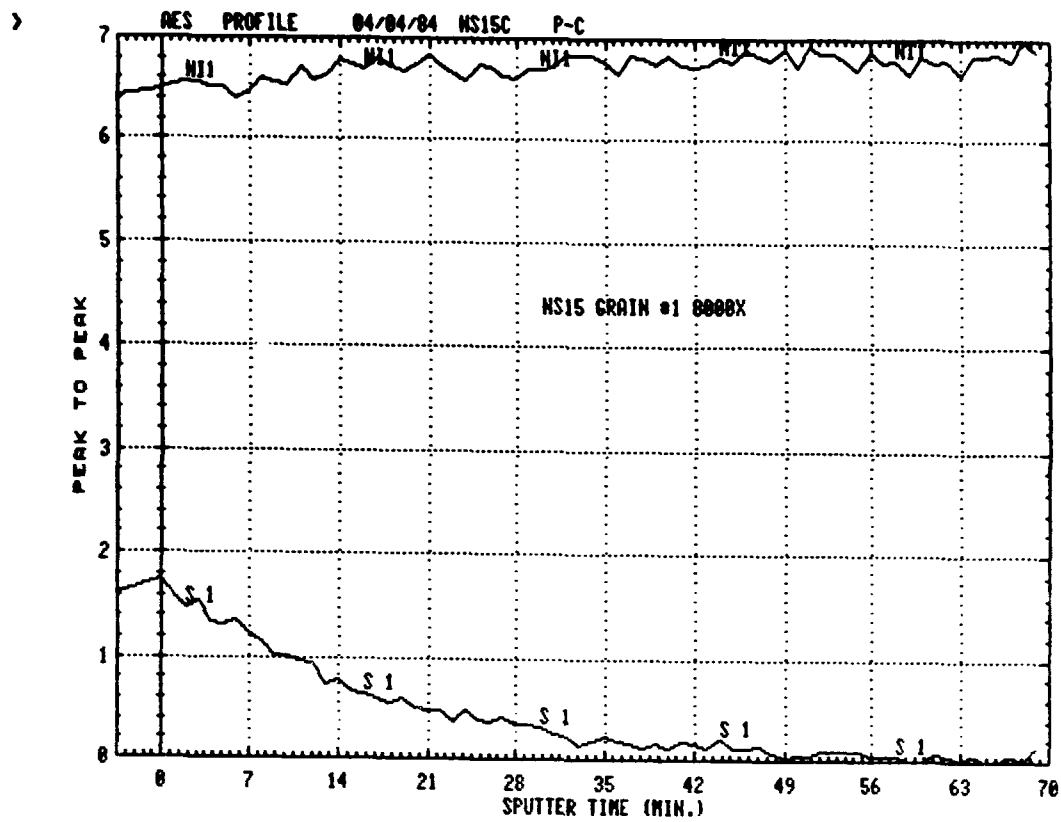sputtering.

AES PROFILE 04/04/84 NS15C P-C

NS15 GRAIN #1 8000X

PEAK TO PEAK

SPUTTER TIME (MIN.)

AES SURVEY SF= 13.549, .000 DAT= 5.00 04/04/84 NS15D P-C

NS15 AFTER PROFILE 8000X

D7[N(E)*E]

KINETIC ENERGY, EV

110

Figure B5.   Auger spectra of sample NS2. The sulfur coverage is about the
              same as that detected on sample NS1 (θ = 0.06).

Figure B6.   Results of depth profiling sample NS2. The depth of sulfur is on
              the order of 50 Å based on the sputtering time required to reduce
              the sulfur signal.

AES   SURVEY   SF= 11.011, .000 DAT= 5.10   05/10/84 NS2A   P-C

SAMPLE NS2 VACUUM FRACTURE BEFORE SPUTTER   1000X

AES   PROFILE   05/10/84 NS2C   P-C

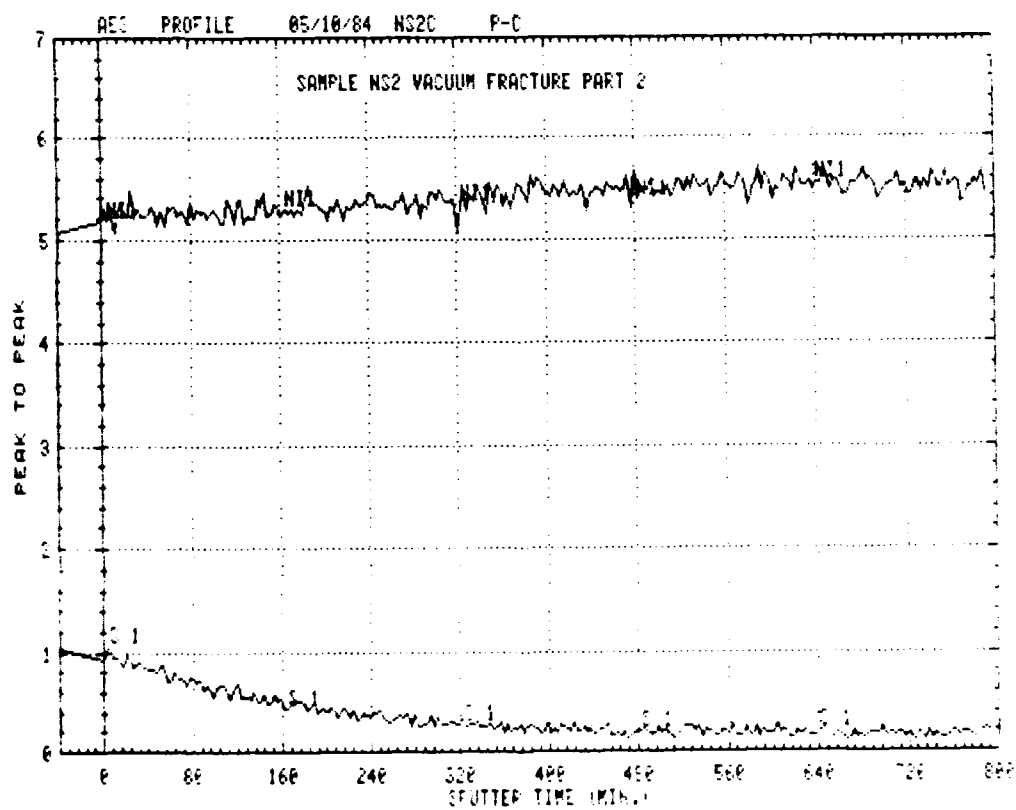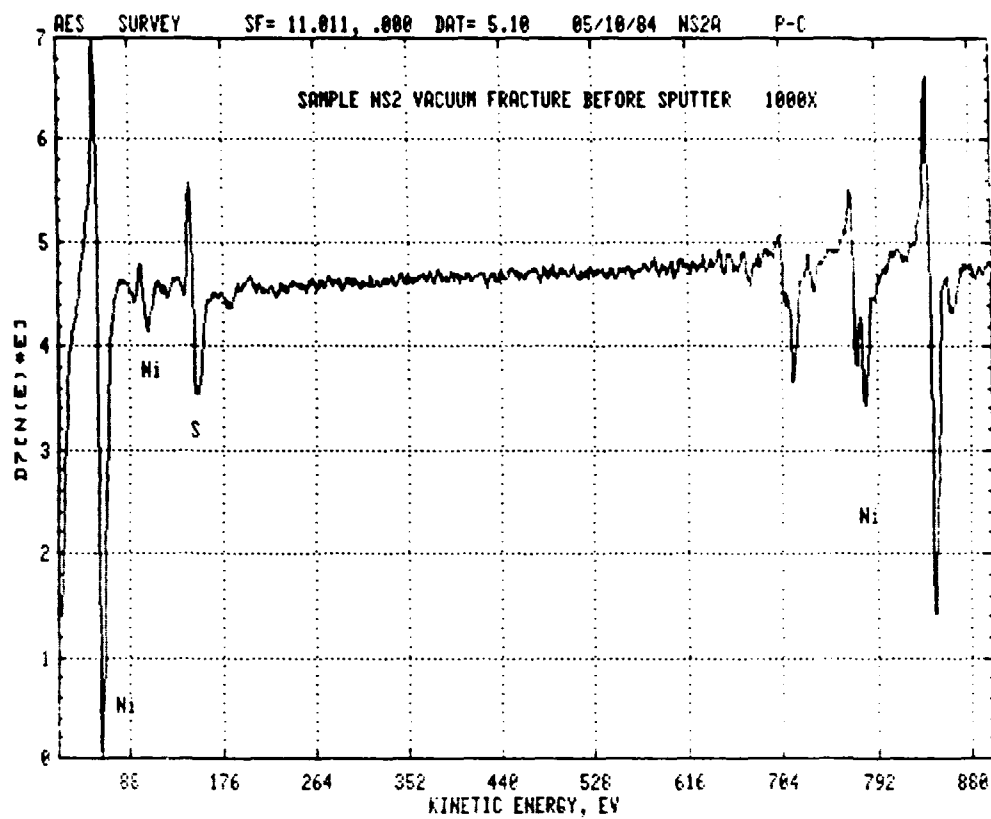SAMPLE NS2 VACUUM FRACTURE PART 2
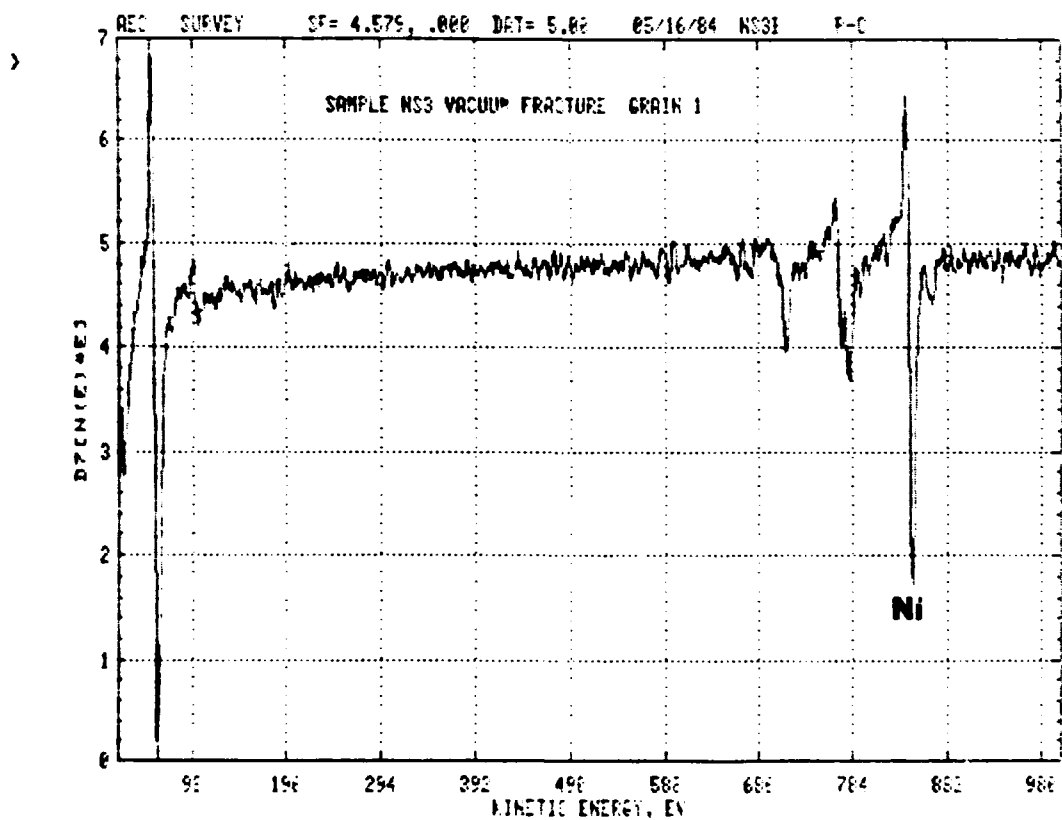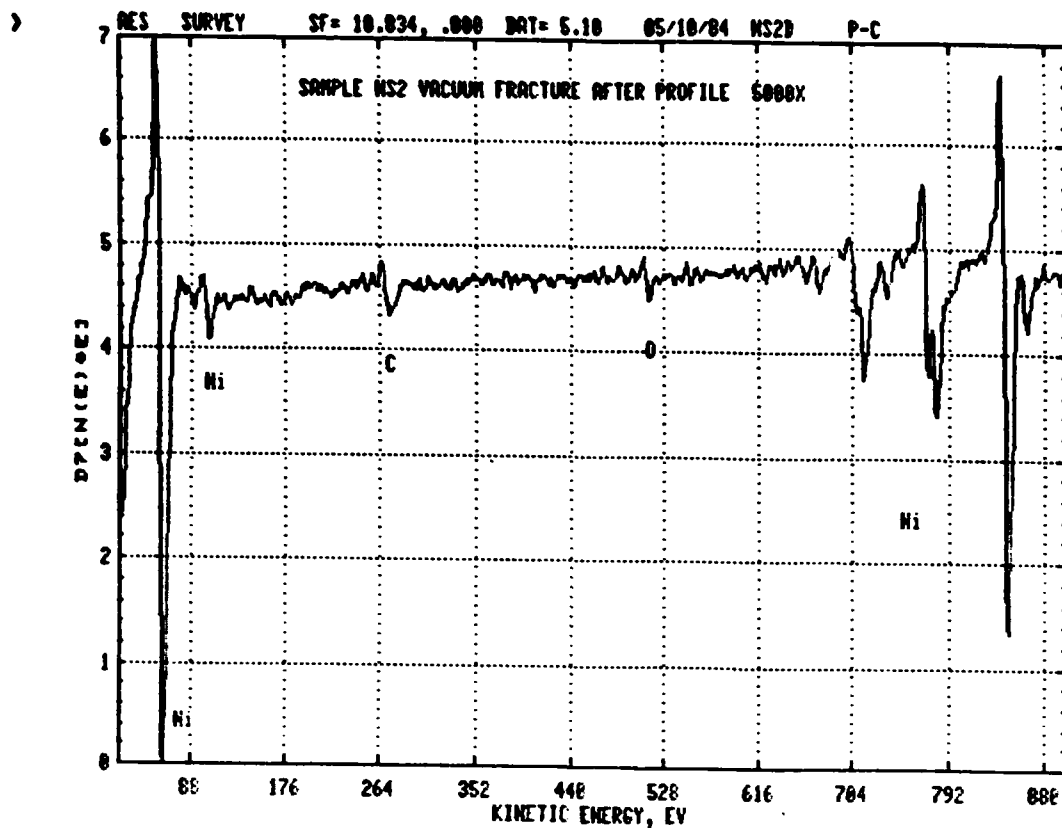
Figure B7.   Auger spectra of sample NS2 after sputtering. The sulfur signal
             has been eliminated.

Figure B8.   Auger spectra of sample NS3 which was fractured in situ. There is
             no indication of elements other than nickel in the spectra.

SAMPLE NS2 VACUUM FRACTURE AFTER PROFILE 5000X

SAMPLE NS3 VACUUM FRACTURE GRAIN 1

Appendix C

This appendix deals with the two assumptions made in applying the McLean equation (equation 7) to the data presented in Figure 11 to calculate the binding enthalpy of hydrogen to nickel grain boundaries; 1) that the reduction of hydrogen in the bulk that occurs during aging is not significant and 2) that the bulk hydrogen concentration has no intrinsic effect on intergranular fracture.

C.1

Reduction of the bulk hydrogen concentration will occur during aging by outgassing from the specimen surface and by loss to traps at grain boundaries and traps within the bulk. Estimates of losses due to these mechanisms will be made in this section. It is determined that the major contribution to reduction of bulk hydrogen concentration is due to segregation at grain boundaries and that under the worst circumstances this reduction will not appreciably affect the analysis performed in this work.

C.1.1 Outgassing

The specimens used in this study were in a highly supersaturated state with respect to solute hydrogen during aging at 45°C, -20°C and -65°C. Due to the mobility of hydrogen at these temperatures, equilibrium will be attained via hydrogen diffusion to and desorption from the nickel surface. Desorption of hydrogen from the surface is probably not the rate controlling step since the permeation activation energy is equal to the sum of the activation energy for diffusion and the heat of solution[29] thus indicating that surface

desorption is not the rate limiting step. Assuming that outgassing is limited
by diffusion of hydrogen to the specimen surface the significance of the loss
of hydrogen can be estimated by considering the rms diffusion distance of a
solute atom which is given by the following expression[49]:

$$\bar{x} = 2.5 \sqrt{Dt} \qquad \text{(C1)}$$

The values of $\bar{x}$ given in the following table were calculated by substituting
the appropriate value of D and using the critical aging time for t for the
three aging temperatures.

Table C.1

RMS Diffusion Distances

$T_{age}(°C)$	$\bar{x}$ (μm)
45°	13
-20	14
-65	13

Since the rms diffusion distance during aging is almost three orders of
magnitude less than the thickness of the specimens used, it is concluded that
the potential for substantial loss of hydrogen by outgassing is small and of
no consequence except for times far exceeding t_c.

C.1.2 Loss to Internal Traps

The reductions in the bulk hydrogen concentration due to trapping at
crystal defects (point, line and planar) are considered in this section. The
deleterious effect of these traps will depend on the binding enthalpy of
hydrogen to the traps and the density of the traps.

a) Point Defects

A variety of point defects exist in the test material during aging that can act as relatively strong hydrogen traps eg. vacancies and impurity atoms. The equilibrium concentration of vacancies at the higher and lower charging temperatures (1150°C and 850°C) used in this work is about 10 ppm and 1 ppm[50]. The binding enthalpy of hydrogen to a vacancy (ΔH_{vac}) has been determined to be about -0.05 eV[44]. The fractional loss of bulk hydrogen concentration due to trapping at vacancies may be given by the following expression assuming the probability of finding a hydrogen atom trapped is given by a Boltzmann distribution and the bulk hydrogen concentration is not reduced appreciably.

$$\text{fractional loss} = C_{vac} \exp \frac{-\Delta H_{vac}}{kT_{age}} \qquad (C2)$$

Substituting the appropriate values, the loss at the lowest aging temperature (-65°C) is about 0.02%, which is insignificant.

The total concentration of impurities for Ni-xx material deduced from Table 1 is about 60 ppm. The question of how much hydrogen is tied up by these elements is difficult to answer because of the lack of information concerning the binding enthalpy of hydrogen to the various impurities reported to be in the test material (Table 1). The trapping strength of an impurity will have two contributions, chemical and mechanical which results from the chemical affinity of hydrogen to the impurity and the strain field in the matrix respectively. The trapping of hydrogen to some impurities in fcc material is generally low, on the order of 0.10 eV[46]. As an approximation it will be assumed that the binding enthalpy to impurity elements is 0.10 eV. The fractional loss of bulk hydrogen concentration due to trapping

c) Loss to Grain Boundaries

The loss of bulk hydrogen concentration due to segregation to grain boundaries may be estimated by considering the average volume of a grain and the volume of grain boundary that it supplies hydrogen to. The geometry of a grain in the test material can be approximated by a sphere with a diameter of 800 μm with a volume equal to $\frac{1}{6}\pi$ (800 μm)^3. The volume of grain boundary region with an enhanced concentration of hydrogen can be taken to be the product of the surface area of the grain boundary sphere and half the depth of the enhanced region. The percent loss of hydrogen will then be given by the following expression

$$\text{fractional loss} = \frac{6 \, d \, \alpha}{D} \tag{C5}$$

where α is the grain boundary enhancement factor and D is the grain diameter.

By taking the hydrogen-grain boundary enthalpy to be the value determined in this work (0.12 eV) and assuming the value of d to be 350 Å, the percent reduction of bulk hydrogen concentration will be 14, 2.8 and 1.2 percent at the aging temperatures -65°C, -20°C and 45°C respectively. Of the contributions to the reduction of bulk hydrogen concentration considered, the loss to grain boundaries is by far the most severe, particularly at the aging temperature of -65°C. However it is not expected that this maximum percent loss will appreciably affect the analysis performed in this work since other errors and scatter of the data is of the same order at -65°C and losses at the higher aging temperatures are insignificant.

C.2 Effect of Bulk Hydrogen Concentration on Fracture Mode

To determine the binding enthalpy between hydrogen and nickel grain boundaries it was necessary to assume that the various levels of bulk hydrogen concentration in the thermally charged samples had no intrinsic effect on the fracture mode i.e. unsegregated hydrogen did not play a role in an inter-granular fracture mechanism. It has been suggested that the effect of hydrogen on the general deformation of charged nickel, an increased propensity for planar slip[9], will enhance the intergranular fracture mode due to an increase in micro stress concentrations at grain boundaries[2,51]. However the effect of hydrogen on planar slip of nickel occurs only when hydrogen has sufficient mobility to interact with mobile dislocations. At the test temperature of -196°C hydrogen is essentially immobile, consequently and is not expected to have, nor are there any reports of an effect on general deformation. To confirm this, TEM was performed on hydrogen charged and hydrogen free samples which had both been deformed to about 35 percent elongation[52]. The results of this study gave no indication that hydrogen had any effect on resulting dislocation character, density or cell size. Thus it is not expected that the levels of bulk hydrogen concentration used in this study had any effect on intergranular fracture other than to serve as a source of hydrogen for segregation to grain boundaries.

120

References

1) T. Boniszewski and G. Smith, Acta Met. 11: 165 (1963)

2) B. Wilcox and G. Smith, Acta Met. 13: 331 (1965)

3) B. Wilcox and G. Smith, Acta Met. 12: 371 (1964)

4) A. Windle and G. Smith, Metal Science Journal 2: 187 (1968)

5) A. Windle and G. Smith, Metal Science Journal 4: 136 (1970)

6) F. Heubaum, Master's Thesis, Univ. of Ill.

7) H. Fukushima and H. Birnbaum, Acta Met. 32: 851 (1984)

8) M. Hagiwara and J. Chene, submitted to Scripta Met.

9) M.R. Louthan, Jr. et al. Material Science and Engineering 10: 357 (1972)

10) C. Loier and J. Boos, Met. Trans. 12A: 1223 (1981)

11) T. Matsumoto and H. Birnbaum, Hydrogen in Metals Proceedings of the Second J.I.M. International Symposium, Transactions of the Japan Institute of Metals Supplement 21: 493 (1980)

12) R. Latanision and H. Opperhauser, Jr., Met. Trans. 3: 483 (1974)

13) T. Miyahara, D.A. Reed and H.K. Birnbaum, Preprint Univ. of Ill., 1983

14) M. Kamdar, Second International Congress of Hydrogen in Metals 3D 10 (1977)

15) W. Chandler, R. Walter, C. Moeller and H. Carpenter, Plating and Surface Finishing, May 1978

16) G.C. Smith, Hydrogen in Metals, I.M. Bernstein and A.W. Thompson eds; ASM, Metals Park, pp. 485-511 (1974)

17) A. Szummer, A. Janko and J. Pielaszek, Bulletin de l'Academie Polonaise des Sciences XIX: 33 (1971)

18) H. Birnbaum, Environment Sensitive Fracture of Engineering Materials, Z.A. Foroulis, ed., The Metallurgy Society of AIME, Warrendale, PA, 362 (1979)

19) C.M. Wayman and G. Smith, Acta Met. 19: 227 (1971)

20) C.M. Wayman and G. Smith, J. Phys. Chem. Solids 32: 103 (1971)

21) I. Bernstein, Mat. Sci. and Eng. 6: 1 (1970)

22) J. Tien, A. Thompson, I. Bernstein and R. Richards, Met. Trans. 7A: 821 (1976)

23) E. Steigerwald, F. Schaller and A. Troiano, Trans. Met. Soc. AIME, 218: 832 (1960)

24) C.D. Beachem, Met. Trans. 3: 437 (1972)

25) J. Eastman, T. Matsumoto, N. Narita, F. Heubaum and H. Birnbaum, Third International Conference on the Effects of Hydrogen on Behavior of Materials, A. Thompson and I. Bernstein, eds. The Metallurgical Society of AIME (1981)

26) S. Lynch, Scripta Met. 13: 1051 (1979)

27) W. Wei, Ph.D. Thesis, Metallurgy Dept., Univ. of Ill. (1983)

28) P. Cotterill, Progress in Metal Physics, Pergamon Press (1961)

29) W. Robertson, Z. Metallkde 64: 436 (1973)

30) P. Bastien and P. Azou, Proceeding First World Metallurgical Congress, ASM, 535 (1951)

31) J. Donovan, Met. Trans. 7A 1677 (1976)

32) J. Hirth and J. Lothe, Theory of Dislocations, McGraw-Hill, New York (1968)

33) J. Weertman and J. Weertman, Elementary Dislocation Theory, Macmillan, New York (1964)

34) Lozinskiy et al., Russ. Metall. 5: 65 (1967)

35) R.A. Mulford, Treatise on Materials Science and Technology, Vol. 25, Academic Press (1983)

36) W.C. Johnson et al., Scripta Met. 8: 871 (1974)

37) T. Miyahara et al. Preprint, Univ. of Illinois (1983)

38) S.M. Bruemmer, Scripta Met. 14: 137 (1980)

39) R.H. Jones et al., Met. Trans. 14A: 1729 (1983)

40) K.S. Sain and M. Meshii, Scripta Met. 17: 1121 (1983)

41) N. Barbouth and J. Ovdar, C.R. Acad. Sc. Paris, t. 269 1618 (1969)

42) W.R. Wampler et al., Philosophical Magazine 34: 129 (1976)

43) D. McLean, Grain Boundaries in Metals, Oxford at the Claredon Press (1957)

44) E.D. Hondros and M.P. Seah, International Metals Reviews, Dec. (1977)

45) M.I. Baskes, Hydrogen Effects in Metals, eds. I.M. Bernstein and A.W. Thompson, AIME-TMS Warrendale, PA, 67 (1980)

46) G.J. Thomas, Hydrogen Effects in Metals, eds. I.M. Bernstein and A.W. Thompson, AIME-TMS Warrendale, PA, 77 (1980)

47) W.M. Robertson, Met. Trans. 10A: 485 (1979)

48) A.W. Thompson and B.A. Wilcox, Scripta Met. 6: 689 (1972)

49) P. Shewmon, Diffusion in Solids, McGraw Hill, New York (1963)

50) A. Seeger and H. Mehrer, Vacancies and Interstitials in Metals, Interscience, New York (1970)

51) D. Smith, Hydrogen in Metals, Univ. of Chicago Press, Chicago (1948)

52) Private communication, G. Bond, Univ. of Illinois (1984)

END

FILMED

1-85

DTIC